Scilight

Power Electronics Research and Applications Transactions

https://www.sciltp.com/journals/perat

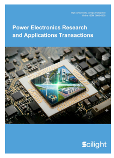

Review

An Overview of Wireless Motor Drive: From Cascaded Structure to Integrated Structure

Xin Felix Chen [1], Yangbin Zeng [2,*], Chi K. Tse (IEEE Fellow) [1], C. Q. Jiang [1], Qianhong Chen [3] and Ching-Ming Lai [4]

[1] Department of Electrical Engineering, City University of Hong Kong, Hong Kong
[2] School of Electric Power, South China University of Technology, Guangzhou 510640, China
[3] Aero-Power Sci-Tech Center, Nanjing University of Aeronautics and Astronautics, Nanjing 210016, China
[4] Department of Electrical Engineering, National Chung Hsing University, Taichung 402, Taiwan
* Correspondence: epybzeng@scut.edu.cn

How To Cite: Chen, X.F.; Zeng, Y.; Tse, C.K.; et al. An Overview of Wireless Motor Drive: From Cascaded Structure to Integrated Structure. *Power Electronics Research and Applications Transactions* **2026**, *1*(1), 1.

Received: 15 June 2026
Revised: 25 July 2026
Accepted: 28 July 2026
Published: 4 August 2026

Abstract: Wireless motor drive (WMD) systems have been developed to address the problems of wire twists and motion limitations. Among various techniques, inductive power transfer (IPT)-based WMD systems have been widely adopted due to their high efficiency and power capacity. This review focuses on the circuit topologies and operating principles of IPT-based WMD systems. Existing WMD systems are categorized into two main architectures: cascaded and integrated structures. In cascaded structures, the IPT converter and the motor drive are implemented as separate stages. In contrast, integrated structures combine IPT and motor drive functions, typically through the use of multiple coils or matrix converters. The paper first examines various cascaded configurations, classified according to the voltage and current characteristics of the IPT output and the motor drive input. A comparative analysis between these topologies is then provided. Subsequently, the paper explores integrated structures, summarizing feasible multi-coil configurations and explaining the multiple frequency operation principle which is essential to such designs. Moreover, the application of matrix converters in WMD systems is reviewed, with a detailed discussion of their modulation strategies. Finally, based on the current state of research, the paper outlines existing challenges and proposes prospective directions for future development in the field.

Keywords: cascaded structure; integrated structure; matrix converter; multi-coil; wireless motor drive

1. Introduction

The rapid development of wireless power transfer (WPT) has accelerated its widespread use in various applications, such as electric transportation [1–3], biomedical implants [4–6], consumer electronics [7–9], industrial equipment [10–12], etc. Among these applications, electric vehicles (EVs) have attracted a great deal of attention. Static and dynamic wireless EV charging systems are commonly considered. In static charging, the battery is usually the terminal load for the WPT converter. However, in the dynamic scenario, the battery is primarily used as a medium of storage for the motor drive. Moreover, batteries may introduce additional losses, and the limitations of battery life and size will affect the system's reliability and power density [3].

As a result, a wireless direct motor drive system for EVs has been proposed [13–17], where the battery is eliminated. In the rest of the paper, wireless motor drives (WMDs) refer to wireless direct motor drives, without being specific. Apart from EVs, wireless motor drives [18–54] have also been applied to other applications, such as high-speed trains [29], piping networks [31,32], robotic arms [30,35], etc. Wireless motor drives can effectively address battery limitations and solve wire twist or slip ring friction problems.

1.1. Wireless Power Transfer

Obviously, the WPT technique is crucial for wireless motor drive systems. Several WPT methods have been developed [2], such as inductive power transfer (IPT), capacitive power transfer, optical power transfer, etc. Among these methods, IPT stands out for its high power and high efficiency properties, making it particularly suitable for wireless motor drive applications. As a result, existing research on wireless motor drives has centered around the IPT technique. This review also focuses on the IPT-based wireless motor drive systems.

In wireless motor drive applications, there are basically rotating and sliding mechanisms [10]. Consequently, the magnetic couplers can also be classified as rotating [55–73] and sliding structures [74–87]. Typical rotating and sliding magnetic couplers are provided in Tables 1 and 2, respectively.

Table 1. Typical rotating magnetic couplers.

Structure	Rotating Speed	Coupling Ability	Cost
Face to face [56–58]	Medium	Low	Low
Coaxial [56,58]	Low	Medium	Low
Detached core [62,63]	High	High	Medium
Double stator [64,65]	High	High	Medium
LL [66,67]	Medium	Medium	Low
LL-delta [68]	Medium	High	Medium
Nested coil [59–61]	Low	Medium	Medium
Extended coil [69]	Medium	Medium	Medium
Three-phase [70–73]	Low	Medium	High

Table 2. Typical sliding magnetic couplers.

Structure	Rotating Speed	Coupling Ability	Cost
U-shape [29,74,75]	High	Low	Low
W-shape [29]	High	Low	Low
I-shape [76]	Medium	Low	Medium
S-shape [77]	Medium	Low	Medium
N-shape [78]	Medium	Low	Medium
Mutiple D [79–81]	Low	Medium	Medium
Overlapped DD [82–84]	High	Medium	High
DDQ pads [87]	High	High	High

Due to the symmetric property of the rotating structure, the rotating movement has little effect on the coupler parameters [58]. However, the high-speed rotation imposes strict requirements on the coupler weight. Besides, the air gap in the magnetic couplers will limit the power transfer capability. As a result, existing research on rotating magnetic couplers primarily focuses on weight reduction and coupling improvement.

In contrast, the sliding structure is more prone to parameter variations during movement. Without a battery for energy compensation, the power fluctuation in the system will be severe. This places a stricter requirement on misalignment tolerance for the sliding structure. A direct way to address this issue is to increase material use. However, the coupler weight and cost will correspondingly increase. Therefore, the challenge with the sliding coupler lies in achieving a trade-off between the cost and the anti-misalignment ability.

Notably, both rotating and sliding magnetic couplers operate with a large air gap between their primary and secondary sides. To address the low coupling coefficient caused by the air gap, compensation networks are usually adopted in wireless power transfer systems.

Primary-side parallel compensation topologies, such as parallel/series (P/S), parallel/parallel (P/P), and parallel-series/series (PS/S) [88,89], require a current source input, which is not convenient in practice. Therefore, the primary-side parallel compensation topologies are not highlighted in the paper. Besides, to maintain a focused exposition, we only discuss compensation topologies involving up to three additional passive components on each side.

Commonly used compensation topologies are summarized in Table 3, where the design principle aims to simultaneously achieve the load-independent output and zero-phase angle properties.

The load-independent output can be either a voltage or a current type. As shown in Figure 1, the load-independent voltage (LIV) compensation includes series/parallel (S/P), series/series-parallel (S/SP), LCC/series (LCC/S), and series/LCC (S/LCC) [90–93]. The S/P compensation can be obtained by removing capacitor C_2 from the S/SP compensation. The S/LCC compensation is the symmetric form of LCC/S. Simpler structures such as LCL/S and S/LCL can be derived by removing C_1 or C_2 from LCC/S or S/LCC respectively. However, the inclusion of C_1 or C_2 allows for increased design flexibility and power transfer capability, so the LCC-based compensation is preferred.

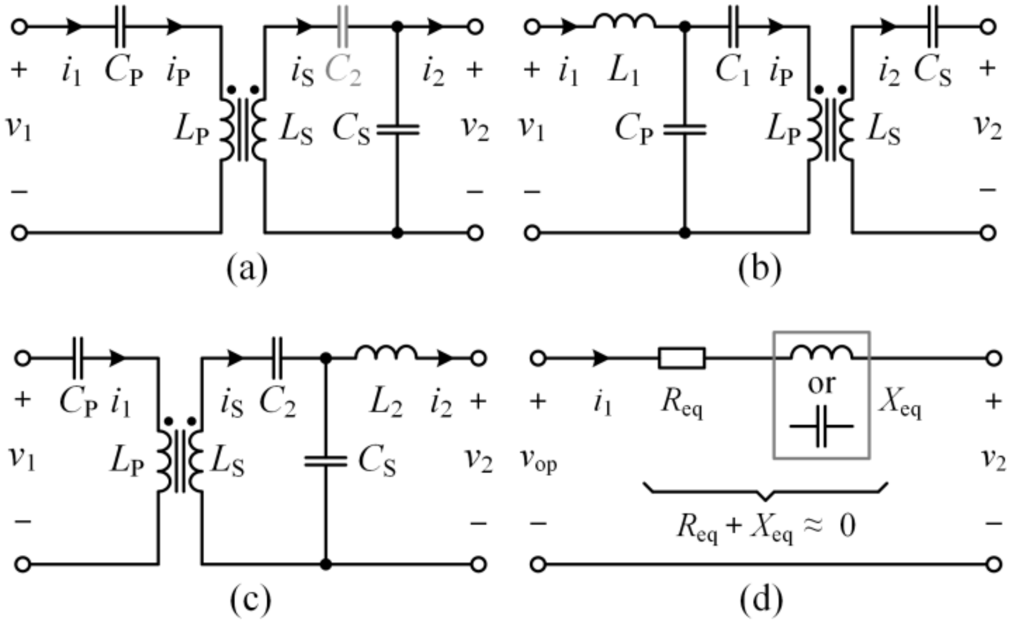

Figure 1. LIV compensation topologies. (**a**) S/SP; (**b**) LCC/S; (**c**) S/LCC; (**d**) Thevenin equivalent circuit.

Table 3. Typical compensation topologies.

LIV	Design Principle
S/P [90]	$\omega_0^2(L_P - \frac{M^2}{L_S})C_P = \omega_0^2 L_S C_S = 1$
S/SP [91]	$\omega_0^2 L_{\sigma P} C_P = \omega_0^2 L_{\sigma S} C_2 = \omega_0^2 n^2 L_M C_S = 1$
LCC/S [92]	$\begin{cases}\omega_0^2 L_1 C_P = \omega_0^2 L_S C_S = 1 \\ \omega_0^2 (L_P - L_1) C_1 = 1\end{cases}$
S/LCC [93]	$\begin{cases}\omega_0^2 L_P C_P = \omega_0^2 L_2 C_S = 1 \\ \omega_0^2 (L_S - L_2) C_2 = 1\end{cases}$
LIC	**Design Principle**
S/S [5,94,95]	$\omega_0^2 L_P C_P = \omega_0^2 L_S C_S = 1$
LCC/P [96]	$\begin{cases}\omega_0^2 L_1 C_P = \omega_0^2 L_S C_S = 1 \\ \omega_0^2 (L_P - L_1 - \frac{M^2}{L_S}) C_1 = 1\end{cases}$
LCC/LCC [97]	$\begin{cases}\omega_0^2 L_1 C_P = \omega_0^2 L_2 C_S = 1 \\ \omega_0^2 (L_P - L_1) C_1 = \omega_0^2 (L_S - L_2) C_2 = 1\end{cases}$

Although S/S compensation can also be designed with LIV properties, it cannot achieve a zero-phase angle in this case [5]. Therefore, S/S compensation is typically designed with load-independent current (LIC) properties [94,95]. Another commonly used LIC compensation is LCC/LCC [97], as shown in Figure 2b. Moreover, by removing L_2 and C_2 from the LCC/LCC compensation, LCC/parallel (LCC/P) compensation can be obtained [96].

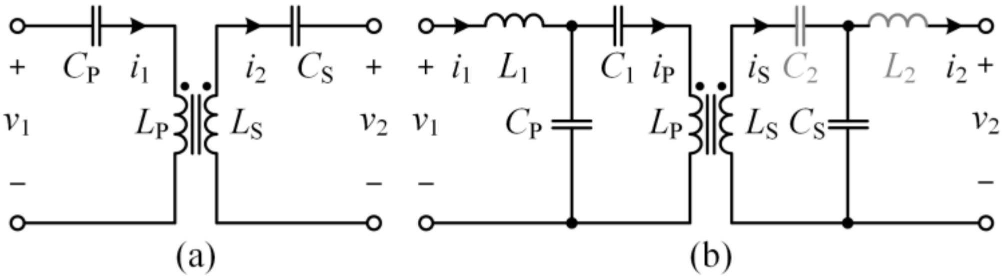

Figure 2. LIC compensation topologies. (**a**) S/S; (**b**) LCC/LCC.

1.2. Motor Drive

Motor drive is another critical component in the system. For DC motors, various DC-DC converters can be employed as motor drives. Notably, the armature voltage does not require a constant DC value, and a square waveform can also be used. The motor speed can be controlled by adjusting the pulse width to regulate the average voltage. In such cases, the half-bridge and full-bridge structures are commonly used.

Figure 3a illustrates a three-phase bridge topology, which is the predominant structure for AC motor drives. This structure supports both sinusoidal and trapezoidal back EMF excitation through appropriate modulation strategies.

For high-power applications, each switch group in Figure 3a can be constructed using series-connected switching devices. However, the two-level output configuration offers little improvement for total harmonic distortion (THD). High-power operation also exacerbates electromagnetic interference (EMI) issues from increased d*v*/d*t* transients. To address these challenges, multilevel topologies, such as the neutral point piloted (NPP) [98], flying capacitor [99], neutral point clamped (NPC) [100], active neutral point clamped (ANPC) [101], cascaded H-bridge (CHB) [102], and modular multilevel converter (MMC) [103], can be considered.

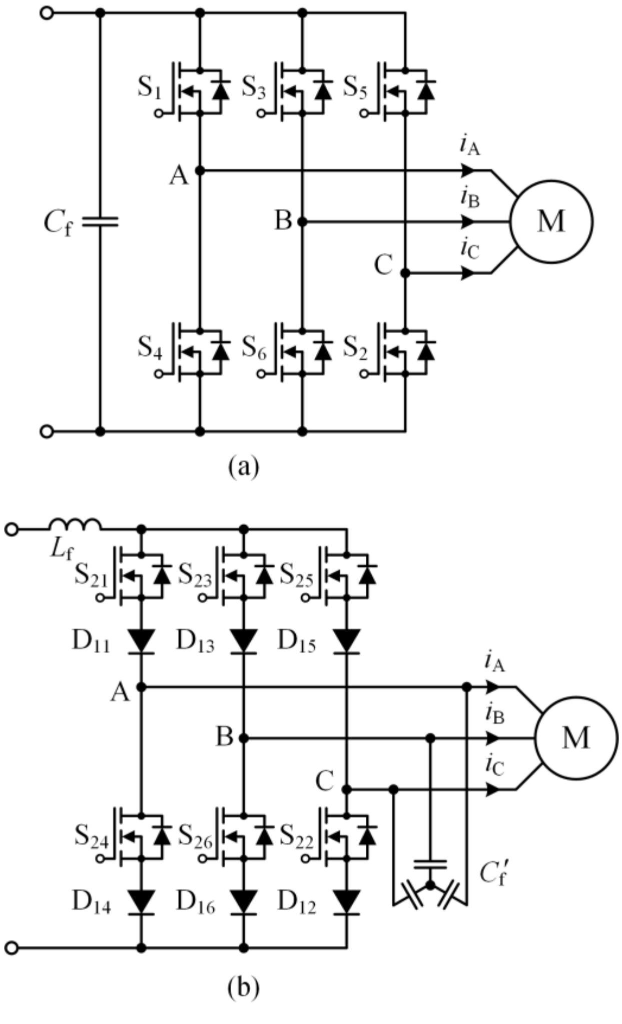

Figure 3. Basic motor drives. (**a**) Voltage source inverter; (**b**) current source inverter.

Besides the above voltage source inverters (VSIs), current source inverters (CSIs) are also effective solutions for motor drives [104], as shown in Figure 3b. Current source converters offer motor-friendly output waveforms and robust short-circuit protection, making them particularly suitable for high-power systems. A key difference between VSIs and CSIs lies in their input components: VSIs utilize a DC-link capacitor, while CSIs require an inductor to establish the current source. The structural difference necessitates switching devices with reverse blocking capability in CSIs. For high-frequency operation, series diode-IGBT or diode-MOSFET pairs are typically used [105], whereas low-frequency applications (below 500 Hz) commonly use symmetrical gate commutated thyristors (GCTs) [106]. In addition, the input inductors in CSIs constrain their dynamic performance. Similar to VSIs, the power rating of CSIs can be increased through series-connected GTC branches.

Unlike other AC motors, switched reluctance motors (SRMs) generate torque independently of current polarity. This characteristic makes standard AC motor drives unsuitable, necessitating the development of specialized converter topologies for SRMs. These topologies are typically categorized into four groups based on the ratio of converter switches and motor phases (n): $2n$-switch, $1.5n$-switch, $(n + 1)$-switch, and n-switch structures [107]. For example, the asymmetric half-bridge converter is the most common $2n$-switch topology [108]. The $1.5n$-switch structure primarily relies on the shared-switch method [109]. The $(n + 1)$-switch structure can be implemented as either a shared switch converter [110] or a C-dump converter [111]. Finally, the n-switch structure is typically realized using an R-dump converter [112] or a split DC capacitor converter [113].

1.3. Wireless Motor Drive

By applying wireless power transfer to motor drives, the wireless motor drive system can be realized, as shown in Figure 4. Both cascaded and integrated structures are feasible options for implementing such a system. In the cascaded structure, the IPT converter and the motor drive are separated by an inductance or capacitance filter. As discussed above, the IPT converter has either LIV or LIC properties [114,115]. Besides, the motor drive can be classified into VSI or CSI structures [106]. As a result, there are four potential combinations of an IPT converter and motor drive. Prior research has primarily focused on the LIV/VSI and LIC/VSI combinations. This review will also encompass the CSI-related combinations. Furthermore, a preliminary comparison among the four configurations will be conducted.

In the integrated structure, the power supply and the motor control functions are merged, resulting in a single power stage and potentially higher efficiency than the cascaded structure. However, the system design will be more complex, and achieving superior motor performance than the cascaded structure can be challenging.

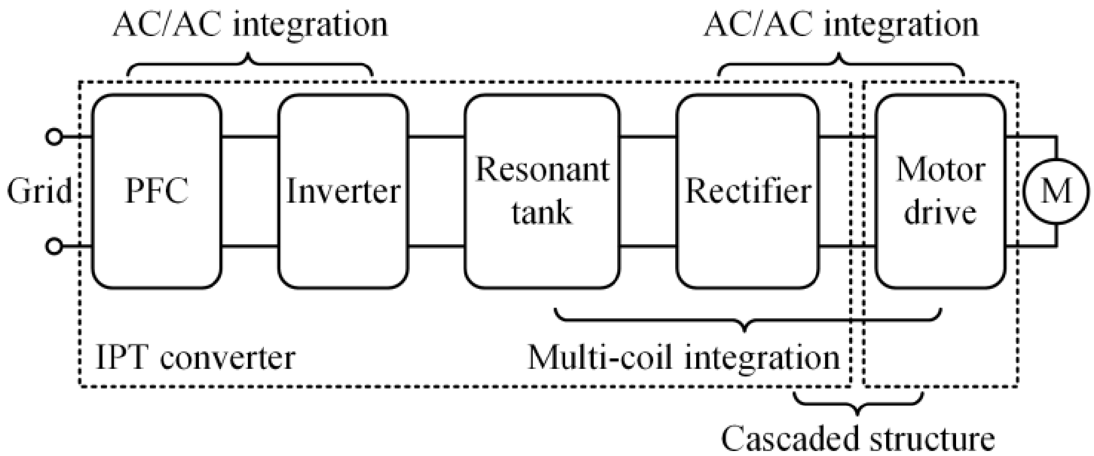

Figure 4. Diagram of wireless motor drive system.

As there are different motor types, such as DC motors [31–40], induction motors (IMs) [41–46], permanent-magnet synchronous motors (PMSMs) [13–28], SRMs [47–52], etc., the integrated structure can also adopt various configurations. The integration can be realized by adding coupling coils or by increasing the number of semiconductor devices. If more coils are used, the derived structure can be seen as copper-based integration. Conversely, if more semiconductor devices are used, the derived structure can be treated as silicon-based integration. In the silicon-based integration, matrix converters are typically adopted to realize direct AC-AC conversion, replacing the conventional two-stage AC-DC-AC approach. As a general principle in power electronics, increasing the use of copper tends to enhance system robustness but reduce power density, whereas expanding the use of semiconductors typically improves power density at the expense of robustness. These general trade-offs also apply to wireless motor drive systems.

Typical parameters of representative wireless motor drive systems are summarized in Table 4. It is seen that existing research primarily focuses on the application of DC motors, PMSMs, and SRMs. For DC motors, the cascaded, multi-coil-based, and matrix converter-based structures are all applicable. For PMSMs, the cascaded and matrix converter-based structures are preferred. For SRMs, the multi-coil-based structure is the most commonly adopted. In terms of compensation topologies, S/S, LCC/S, and LCC/LCC are the most frequently used, with resonant frequencies normally ranging from 85 kHz to 150 kHz. Besides, most research has focused primarily on the unidirectional power flow scenario, with comparatively little work exploring bidirectional power flow. Regarding the transmission distance, existing systems typically operate at a distance of less than 20 cm, with many operating at a short distance of tens of millimeters. Within this distance range, the coupling coefficients of reported prototypes are generally between 0.1 and 0.3. Furthermore, the power levels in existing research are observed to be relatively low, mostly under several hundred watts. Additionally, the system efficiency is relatively low, generally below 90%.

Table 4. Summary of typical wireless motor drive systems.

Motor	Ref.	Structure	Compensation Network	Frequency (kHz)	Bidi. Power [a]	Transmission Distance	*k* [b]	Power	Efficiency
DC	[31]	Cascaded	S/LCLCC	90,130	No	13 cm	0.10	200 W	83.5%
	[36]	Cascaded	LCCC/CCL	30,90	No	10 cm	0.15	180 W	90.0%
	[34]	Multi-coil	LCL/S	130,160	No	13 cm	0.12	180 W	85.0%
	[35]	Multi-coil	S/LCC	85	No	10 cm	0.15	160 W	88.7%
	[40]	Matrix converter	S/CP	200	No	60 mm	0.15	200 W	89.7%
IM	[42] [c]	Multi-coil	LCL/S	109,116	No	30 mm	0.20	110 W	86.2%
	[41] [d]	Matrix converter	S/P	40	No	15 cm	0.10	780 W	NA
PMSM	[14]	Cascaded	S/S	85	Yes	10 cm	0.20	3.3 kW	88.8% [e]
	[18]	Cascaded	S/P	100	No	12 mm	0.52	NA	<60%
	[20]	Cascaded	S/S	100	No	50 mm	0.23	300 W	85.4%
	[22]	Cascaded	LCC/LCC	85	Yes	70 mm	0.24	400 W	80.0%
	[25]	Multi-coil	S/S	89,137	No	24 mm	0.21	40 W	83.0%
	[26]	Multi-coil	S/S	100,150	No	90 mm	0.20	157 W	84.3%
	[27]	Matrix converter	LCC/LCC	85	Yes	10 cm	0.57	1 kW	92.5% [f]
	[28]	Matrix converter	S/S	85	Yes	10 cm	0.26	600 W	93.3%
SRM	[47]	Cascaded	LCC/S	85	No	10 cm	0.18	200 W	82.0%
	[49]	Multi-coil	LCC/S	90,110,130	No	15 cm	0.13	NA	80.0%
	[50]	Multi-coil	S/S	100	No	20 cm	0.08	134 W	89.1%
	[52]	Multi-coil	LCC/S	85,100,115	No	NA	0.22	120 W	83.6%
Step motor	[53]	Multi-coil	LCL/S	85	No	50 mm	0.31	NA	87.5%
BLDC [g]	[54]	Multi-coil	S/S	299-359	No	20 mm	0.25	134 W	80.2%

[a]. Bidirectional power flow; [b]. coupling coefficient; [c]. shaded pole induction motor; [d]. single-phase induction motor; [e]. VSI efficiency is not included; [f]. resonant tank efficiency is not included; [g]. brushless DC motor.

Overall, given the diverse applications of wireless motor drives, system parameters such as switching frequency, transmission distance, and power level vary significantly across existing prototypes to meet different operating requirements. Besides, the performance of existing wireless motor drive systems remains limited, particularly in terms of power level and efficiency. Research on wireless motor drives is still in a relatively early stage, with many challenges lying ahead. To support further progress in this field, this paper provides a comprehensive review of the research area, aiming to clarify key challenges and suggest promising directions for future investigation. This paper is structured around different system architectures, with the remaining sections outlined below. Section 2 presents the structure and operation of cascaded WMD systems. Section 3 reviews multi-coil-based WMD systems. Section 4 discusses matrix converter-based systems. Section 5 outlines prospective research directions. Finally, Section 6 provides a summary of the paper.

2. Cascaded Structure

2.1. System Structure

This section will concentrate on the cascaded circuit structure, which consists of the IPT converter as the front-end stage and the motor drive inverter as the back-end stage [13–22,46,47].

The IPT converter and the motor drive are separated by inductance or capacitance filters. Notably, the decoupled filters vary with the secondary-side compensation topologies. As shown in Figure 5, when series compensation is used on the secondary side, a capacitance filter is necessary. Otherwise, the series compensation component will be ineffective due to the current clamping by the inductance filter. Conversely, when applying parallel compensation on the secondary side, an inductance filter is required to prevent voltage clamping of the parallel compensation component.

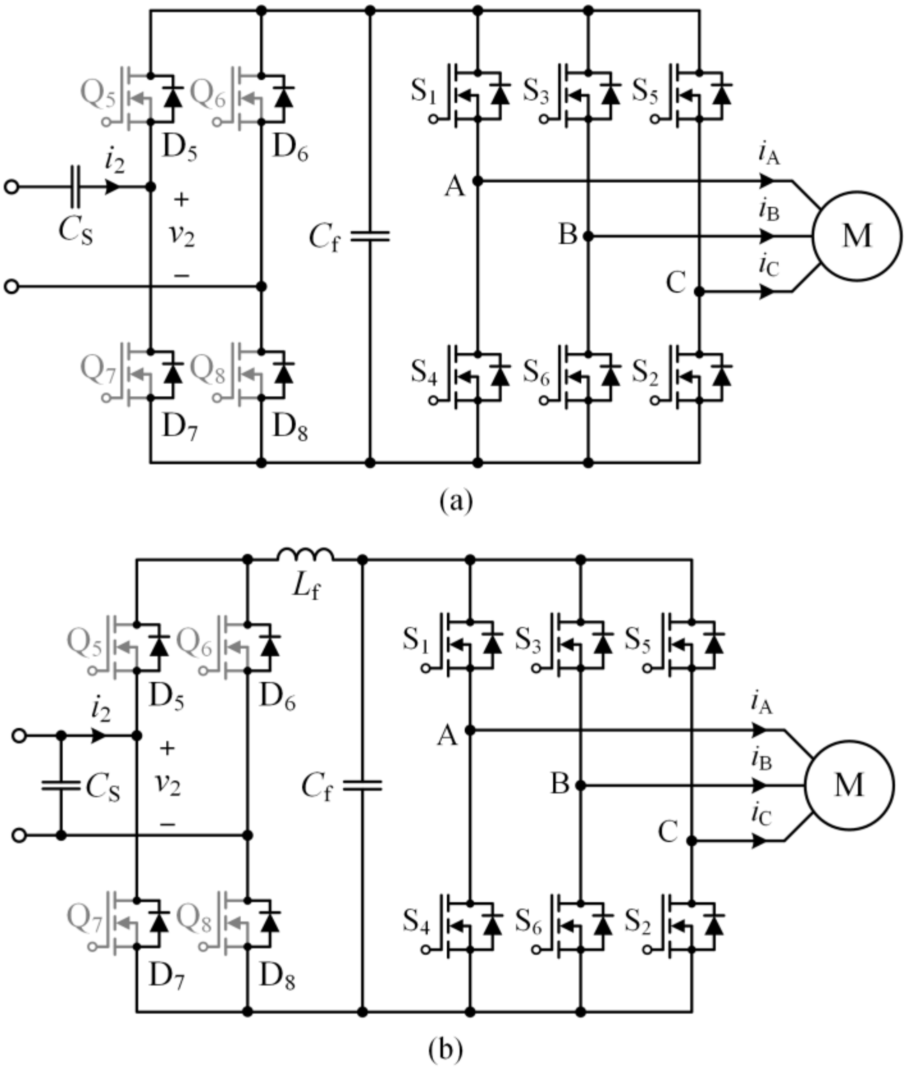

Figure 5. VSI-based wireless motor drive. (**a**) Series compensation on the secondary side. (**b**) parallel compensation on the secondary side.

Similar to IPT converters, motor drives also exhibit voltage and current properties. As shown in Figure 5, the VSI motor drive operates with a voltage source, thus requiring a capacitance filter. On the contrary, as shown in Figure 6, the CSI motor drive relies on a current source input, necessitating an inductance filter. Besides, to maintain an explicit current vector basis and prevent reverse current in the input inductance, a diode should be added in series with each switching device. Moreover, a three-phase capacitance filter is necessary between the inverter and the motor due to the square waveform of the output current. Despite being more complex than the VSI motor drive, the CSI motor drive could effectively avoid shoot-through issues, making it suitable for high-power applications.

It is worth noting that the filters in the IPT converter's output or motor drive's input also serve as storage components. Therefore, these filters typically have a large volume and often adopt electrolytic capacitors. However, the three-phase capacitance filter targets high-frequency harmonics. Thus, the required capacitance is not significant, and highly reliable film capacitors can be used.

Based on the above analysis, employing the VSI motor drive allows us to obtain the LIV/VSI [17–19,47] and LIC/VSI [13–16,20–22,46] structures. Meanwhile, using the CSI motor drive results in the LIV/CSI and LIC/CSI structures. The following discussion will explore the various combinations of IPT converters and motor drives.

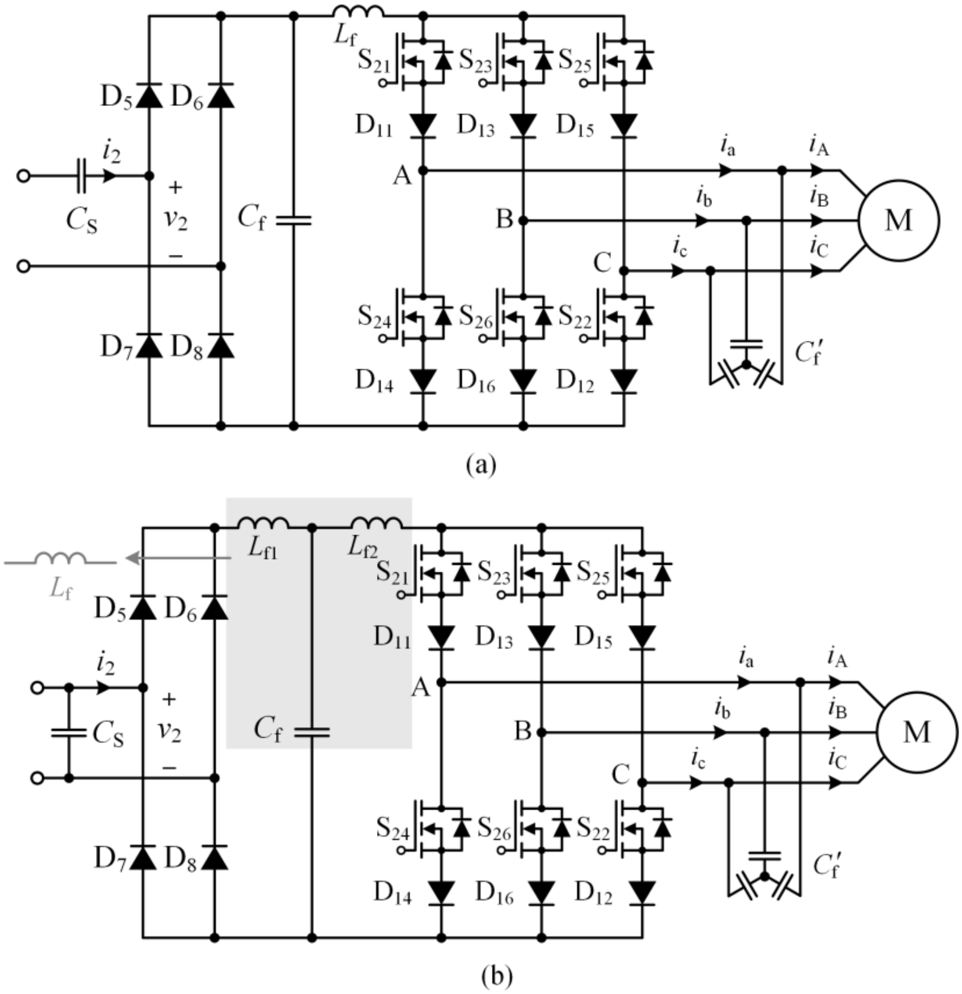

Figure 6. CSI-based wireless motor drive with unidirectional power flow. (**a**) Series compensation on the secondary side. (**b**) parallel compensation on the secondary side.

2.1.1. LIV/VSI Structure

The LIV/VSI structure is shown in Figure 5, with the primary side and resonant tank omitted for brevity. When employing series compensation on the secondary side, a capacitance filter needs to be used as the decoupling component between the IPT converter and the motor drive. On the other hand, secondary-side parallel compensation necessitates the use of an LC filter.

As mentioned before, the misalignment effect is not severe in rotating applications, making it easy to achieve a stable bus voltage with the LIV property. Also, the motor drive inverter can typically tolerate some variation in the bus voltage. As a result, high-frequency wireless communication can be saved. Nevertheless, normal wireless communication remains necessary for command setting or state monitoring, which can be easily realized without requiring a high transmission rate.

For sliding applications, the LIV property of the IPT converter may be lost. The coupler's misalignment ability determines whether high-frequency wireless communication is necessary. If the bus voltage can meet the requirements despite various misalignment positions, high-frequency wireless communication can be saved. Otherwise, high-frequency wireless communication needs to be used.

Furthermore, in the case of unidirectional power flow, only the diode rectifier (D_5–D_8) is required. For bidirectional power flow, the diode rectifier has to be replaced with an active rectifier (Q_5–Q_8). It is noted that more attention needs to be paid to the bidirectional LIV/VSI structure.

First, implementing the dual-bridge control [94,95] becomes challenging when series compensation is used on the secondary side, as shown in Figure 5a. Applying Thevenin's theorem, the LIV compensation can be simplified as a voltage source (v_{op}) and parasitic impedance (R_{eq}, X_{eq}). As the capacitance filter is used, the secondary side is modeled with a voltage source (v_2), as shown in Figure 1d.

For brevity, only the fundamental harmonic components are considered. Assuming $\dot{V}_1$ as the reference and a phase difference of θ between $\dot{V}_1$ and $\dot{V}_2$, we obtain $\dot{V}_1 = \dot{V}_2$ and $\dot{V}_2 = V_2\angle\theta$, where V_1 and V_2 are the amplitudes of $\dot{V}_1$ and $\dot{V}_2$ respectively. Then the input current is given by $\dot{I}_1 = (\dot{V}_1 - \dot{V}_2) / (R_{\text{eq}} + \text{j}X_{\text{eq}})$ and the amplitude is derived as

$$I_1 = \sqrt{\frac{(V_1 - V_2)^2 + 2V_1V_2(1 - \cos\theta)}{R_{\text{eq}}^2 + X_{\text{eq}}^2}}. \tag{1}$$

Around the LIV point, the parasitic parameter $R_{\text{eq}}^2 + X_{\text{eq}}^2$ is very small. As shown in (1), to prevent a large current, both the primary and secondary voltages must have nearly identical amplitudes and phase differences, specifically $V_1 \approx V_2$, $\theta \approx 0$. Besides, switching frequencies of $\dot{V}_1$ and $\dot{V}_2$ must be kept close to avoid an increase in θ.

In practical applications, achieving the above limitations on $\dot{V}_1$ and $\dot{V}_2$ is challenging. Consequently, dual bridge control may result in significant current flow within the system. In this case, the active rectifier needs to operate as a diode rectifier, relying on the body diodes that typically have a large voltage drop. The increased voltage drop will cause higher losses in the system.

If secondary parallel compensation is used in the bidirectional power flow application, as shown in Figure 5b, the situation of two voltage sources in parallel can be avoided due to the inductance filter. However, implementing this configuration remains challenging due to the current spike problem [116].

Ideally, the current spike can be mitigated if the secondary-side voltage v_2 and current i_2 are perfectly aligned. However, there is always a difference between v_2 and i_2 due to control delays and overlap time. As an example, consider the scenario where v_2 leads i_2 as shown in Figure 7b. During the commutation intervals [t_1, t_2] or [t_3, t_4], the parallel capacitor C_S will get shorted by the upper or lower devices, leading to a surge current in the shorted loop. Similar to the CSI motor drive, adding a diode in series with each switching device can prevent the current spike. However, to ensure bidirectional power flow, the additional diodes have to be replaced with switching devices, leading to a significant increase in system cost and control complexity.

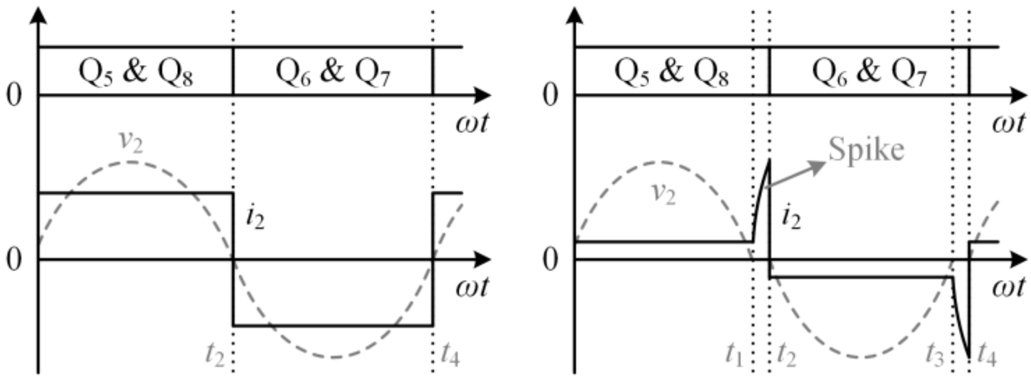

Figure 7. Current spikes in the active rectifier with inductance filter. (**a**) v_2 aligns with i_2; (**b**) v_2 leads i_2.

2.1.2. LIC/VSI Structure

The LIC/VSI structure is similar to the LIV/VSI structure, as shown in Figure 5. However, in the LIC/VSI structure, the bus voltage is highly sensitive to load changes due to its current output characteristic. Therefore, high-frequency wireless communication is typically required, even for rotating applications. Besides, as the current property circuit is controlled to maintain a constant voltage, the dynamic performance of the LIC/VSI structure is inferior to that of the LIV/VSI structure [18].

Nevertheless, the LIC/VSI structure has an advantage in bidirectional power flow applications. When employing series compensation on the secondary side, the system can be represented by a parallel arrangement of a current source and a voltage source, which is easier to be realized [22]. Unfortunately, when parallel compensation is used on the secondary side, the system also finds it hard to operate effectively due to the current spike problem.

2.1.3. LIV/CSI Structure

The LIV/CSI structure is shown in Figure 6. For secondary-side series compensation, a CL filter has to be used as the decoupling component. Meanwhile, secondary-side parallel compensation requires the use of an LCL filter. Moreover, it is possible to simplify the LCL filter with an inductance filter, as only the DC bus current is desired [106].

As discussed above, a stable bus voltage can be easily obtained with the LIV-type IPT converter for rotating movement applications. Then a current source can be obtained by adding an inductance [117]. For a limited load variation, high-frequency wireless communication can also be saved. Nevertheless, the inductance typically needs to be very large to achieve the desired current source property, increasing the system volume and deteriorating the dynamic performance. For sliding movement applications, high-frequency wireless communication is normally inevitable to mitigate the misalignment effect and maintain a stable bus current.

As shown in Figure 8, to enable bidirectional power flow, like the VSI-based structure, the diode rectifier (D_5–D_8) needs to be replaced with an active rectifier (Q_5–Q_8). Moreover, the block diodes (D_{11}–D_{16}) in the CSI motor drive should also be substituted with switching devices (S_{11}–S_{16}). It is observed that the CSI motor drive becomes a single-phase to three-phase matrix converter. Obviously, the CSI-based bidirectional wireless motor drive system is much more complex than the VSI-based system. Furthermore, achieving bidirectional power flow in the LIV/CSI configuration is also challenging due to limitations imposed by either parallel voltage sources or current spikes.

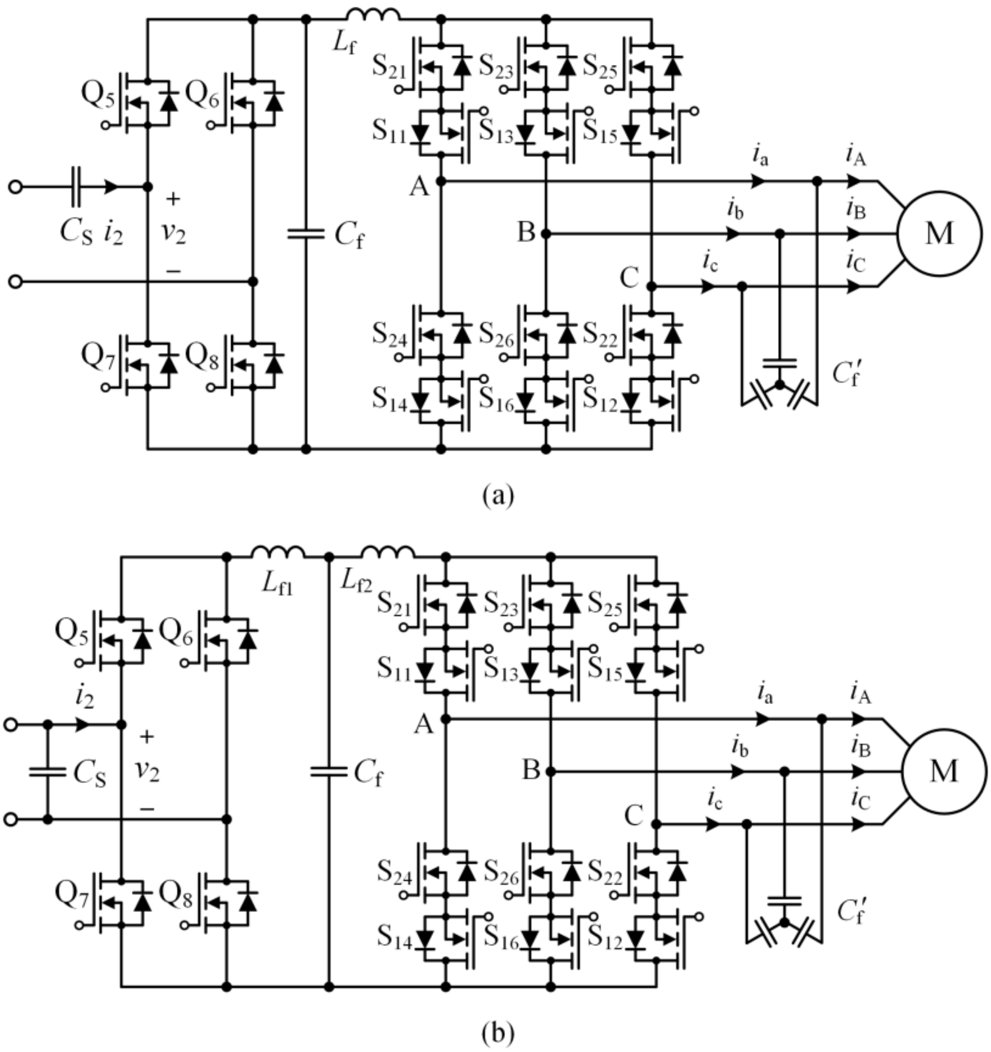

Figure 8. CSI-based wireless motor drive with bidirectional power flow. (**a**) Series compensation on the secondary side. (**b**) parallel compensation on the secondary side.

2.1.4. LIC/CSI Structure

The LIC/CSI structure is similar to the LIV/CSI structure except for the resonant tank. Due to the current compatibility between the IPT converter and the motor drive, high-frequency wireless communication can be saved in rotating movement applications. Whether to use high-frequency wireless communication in sliding movement applications, similar to the LIV/VSI structure, depends on the coupler's misalignment ability. Notably, compared to the LIV/CSI structure, the LIC/CSI configuration allows for a significant reduction in the inductance filter size due to the IPT converter's current property.

Regarding bidirectional power applications, like the LIC/VSI structure, the LIC/CSI configuration can operate effectively with the structure shown in Figure 8a when series compensation is used on the secondary side. However, if parallel compensation is used on the secondary side, as shown in Figure 8b, the LIC/CSI system will experience current spikes.

2.1.5. Discussion

The four typical cascaded structures described above are summarized in Table 5. The high-frequency wireless communication mentioned in the table is specifically for the rotating movement application, as it is usually necessary for all structures in the sliding movement application.

Table 5. Summary of cascaded structures.

Topology	Secondary Compensation	Filter	Wireless Communication	Bidirectional Power
LIV/VSI [17–19]	Series	C	No	Yes
	Parallel	LC	No	No
LIC/VSI [13–16,20–22,46]	Series	C	Yes	Yes
	Parallel	LC	Yes	No
LIV/CSI	Series	CL	No	Yes
	Parallel	L	No	No
LIC/CSI	Series	CL	No	Yes
	Parallel	L	No	No

LIV: load-independent voltage; LIC: load-independent current; VSI: voltage source inverter; CSI: current source inverter.

It is observed that high-frequency wireless communication can be saved when the IPT converter output matches the motor drive type. Besides, it is not advisable to employ parallel compensation on the secondary side for bidirectional power flow applications. Although using series compensation on the secondary side in an LIV-based system allows for bidirectional power flow, it will lead to increased rectifier losses. Moreover, if the CSI motor drive is used for the back-end stage, it is preferable to use LIC compensation regardless of whether the power flow is unidirectional or bidirectional.

2.2. System Operation

The control objective of a cascaded structure is to maintain a stable secondary DC-link voltage (or stable current in CSI-based structures), which can be implemented on the secondary side using an active rectifier [13,14] through hysteresis control. By controlling the active rectifier's switching states, the system alternates between two operational modes: Mode 1 (rectifier mode), in which power is supplied to the load, and Mode 2 (short-circuit mode), where the secondary coil is short-circuited, and power delivery to the load is interrupted. A hysteresis comparator continuously compares the actual value with its reference value. Based on this comparison, the system switches between these two modes to regulate and stabilize the secondary DC-link voltage.

Meanwhile, the primary-side DC-link voltage is dynamically adjusted in response to load demand to guarantee sufficient power transmission [14,15]. Motor speed and torque references are transmitted from the secondary to the primary side via wireless communication, allowing for the calculation of the motor's required power through online loss prediction. Using this estimated power along with known coil parameters, the required primary-side voltage is derived. This value serves as the reference for the primary PFC converter, which in turn regulates the primary inverter output. This feedforward approach can effectively mitigate voltage drops resulting from insufficient power transmission.

Moreover, the maximum power efficiency tracking (MPET) scheme can be used to enhance system efficiency [18]. This scheme dynamically adjusts the secondary DC-link voltage using a perturbation and observation method, while simultaneously monitoring the corresponding input power to identify the optimal operating point. A key advantage of this approach is that it operates without an additional DC/DC converter, thereby reducing system cost and physical size.

Furthermore, to eliminate the need for wireless communication, secondary-side control methods can be used [17,38]. In this approach, the primary-side inverter operates with fixed-frequency and duty-cycle signals, while motor control is handled entirely by the secondary-side converter. The challenge then lies in maintaining a stable secondary side DC-link voltage. Since no wireless communication is used, a stable DC-link voltage is normally guaranteed during the design phase by accounting for all expected load and misalignment ranges.

Meanwhile, as the primary-side inverter does not need to implement the phase-shift or pulse-width modulation (PWM), soft switching can be achieved across a wide operating range [17,38]. Additionally, a stable DC-link voltage does not imply that the voltage is constant. Indeed, the voltage can vary between defined upper and lower limits, which are determined by the motor drive voltage level and isolation requirements. The variable DC-link voltage can be employed to optimize overall system efficiency during the design process [17,21,22].

3. Multi-Coil-Based Structure

In the cascaded structure, the front-end and back-end stages can be designed separately, providing better design flexibility. However, this approach results in an increased power conversion stage. To reduce the conversion loss and improve the system efficiency, several integrated wireless motor drive structures have been proposed. This section will focus on multi-coil-based integrated wireless motor drive systems.

3.1. System Structure

To reduce the power conversion stages, it is desirable for the IPT converter to directly connect to the motor winding. For DC motors [33–36], a direct connection is feasible. However, due to the unidirectional property of the diode, the motor cannot rotate in both directions. As a result, the multi-coil method is applied, as shown in Figure 9a. In this structure, each channel is used to control the motor for one rotating direction [34], then the bidirectional rotation can be achieved. Besides, as shown in Figure 9b, the multi-coil structure can also be used to provide auxiliary power for the motor's exciting winding [33], eliminating extra power supplies on the secondary side.

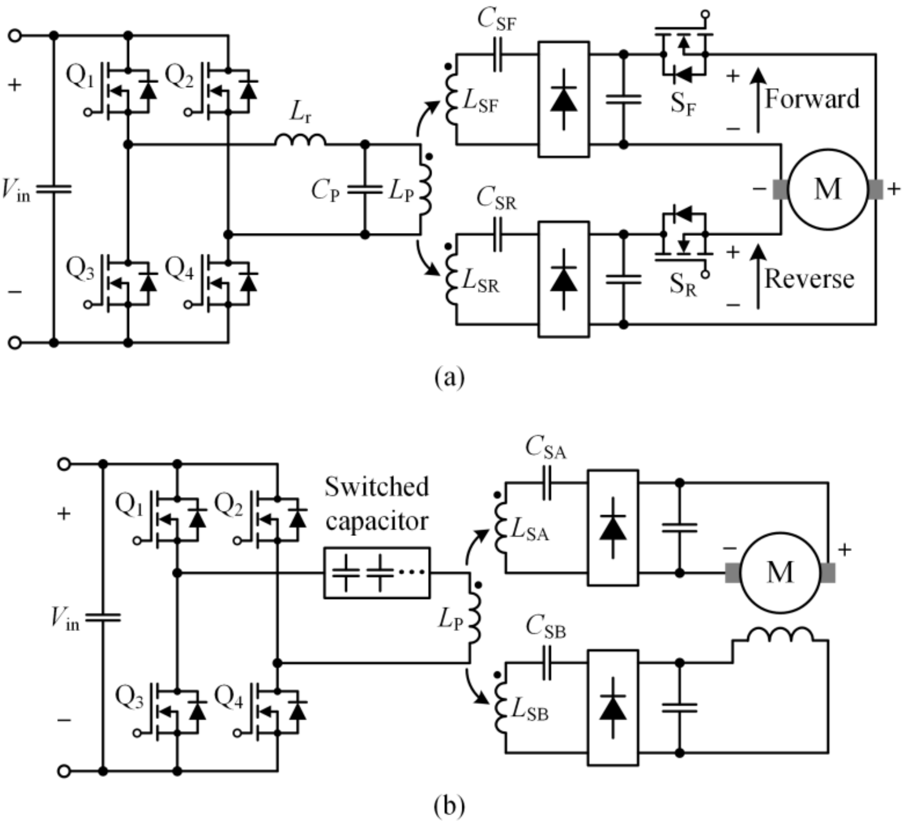

Figure 9. Multi-coil-based integrated wireless DC motor drive. (**a**) Bidirectional rotation; (**b**) auxiliary power for excitation.

Since AC motors typically consist of multiple windings, separate receiver channels are required. Then, the magnetic coupler needs to be built with multiple coils. Besides, the IPT converter typically supplies only DC power. Hence, the multi-channel method is commonly employed for motors requiring square current excitation, such as SRMs [48–52], step motors [53], brushless DC motors [54], etc. Although the multi-channel arrangement can also be applied to motors with sinusoidal current excitation, like the open-winding PMSM [26], each channel requires an additional circuit for wave shaping. As a result, the system cost and complexity will significantly increase.

Figure 10 provides typical multi-coil structures for SRMs. To control the motor rotation, different switching frequencies are selected based on the rotor position. Then each motor winding can be excited sequentially. Figure 10a shows a primary three-coil structure [50]. A three-phase voltage source inverter is used, which actually operates as three half-bridge inverters for the three channels. To increase the power level, three full-bridge inverters should also be used [26].

However, the primary multi-coil structure requires an increase in coil and ferrite use, leading to a more substantial cost increase, particularly as the number of channels increases. To balance the system performance and the cost, the switched capacitor can be used on the primary side [52,118], as shown in Figure 10b. In this structure, the capacitor array is adjusted through the semiconductor devices to make the primary side be in resonant states for different frequencies. The operation principles will be explained in the following part.

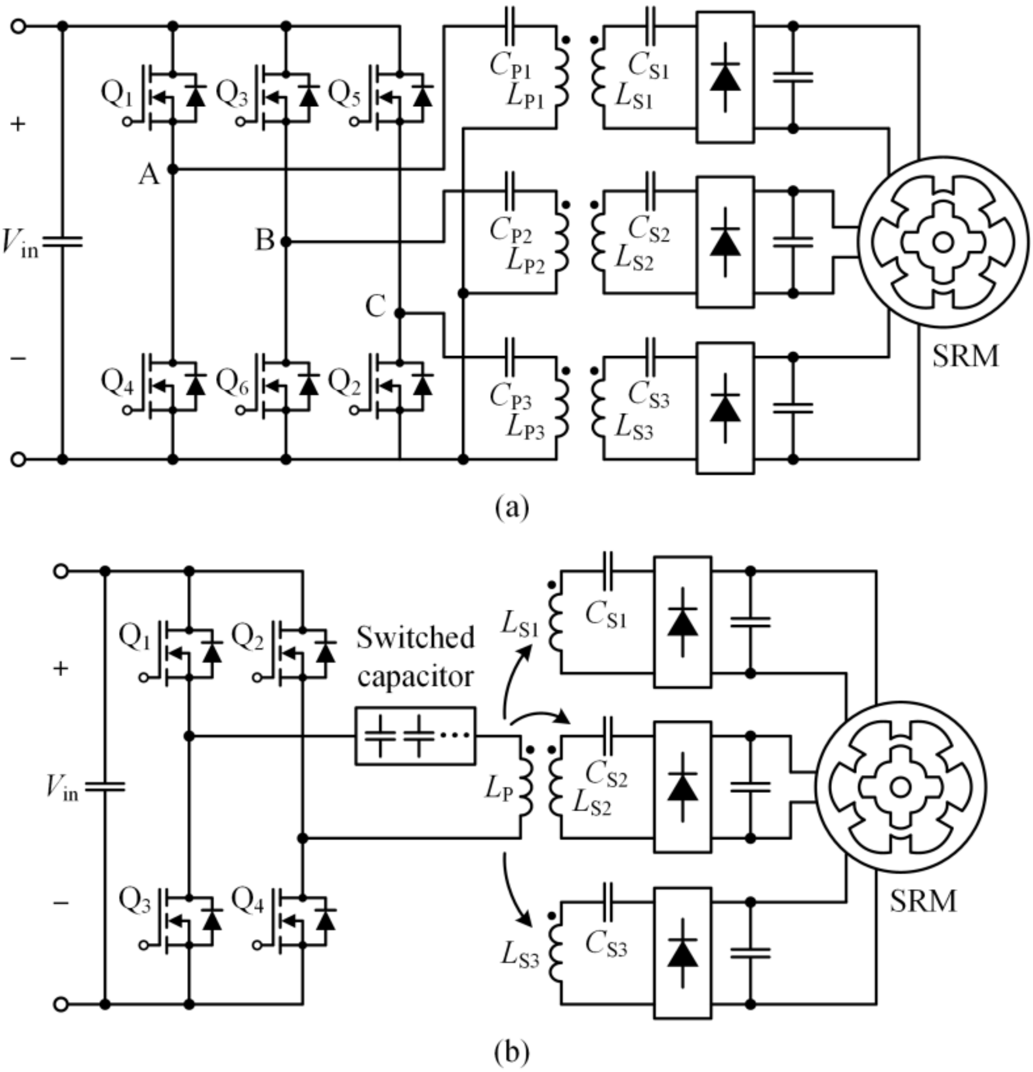

Figure 10. Multi-coil-based integrated wireless SRM motor drive systems. (**a**) Multiple primary-side compensation; (**b**) switched capacitor.

3.2. System Operation

In the multi-coil-based structure, each IPT channel needs to be controlled independently to obtain optimal motor performance. The multi-frequency technique is widely used for this purpose. A simple implementation of the multi-frequency method [34,119] is shown in Figure 11a, using two channels as an example.

Referring to Figure 11a, there is one coil on the primary side and two coils on the secondary side. To realize decoupled power transfer, it is essential to design two receivers with distinct resonant frequencies. Assuming that the resonant frequencies for channel 1 and channel 2 are f_1 (or ω_1) and f_2 (or ω_2) respectively, we can obtain $\omega_1^2 L_{S1} C_{S1} = 1$ and $\omega_2^2 L_{S2} C_{S2} = 1$. Based on the parameters provided in [48], the transconductance curves (i_{S1}/v_P, i_{S2}/v_P) are plotted in Figure 12a. It is seen that i_{S1} is much larger than i_{S2} at frequency f_1 = 110 kHz, while i_{S2} is much larger than i_{S1} at frequency f_2 = 130 kHz. Therefore, by changing the switching frequency between f_1 and f_2, it is feasible to independently control channels 1 and 2.

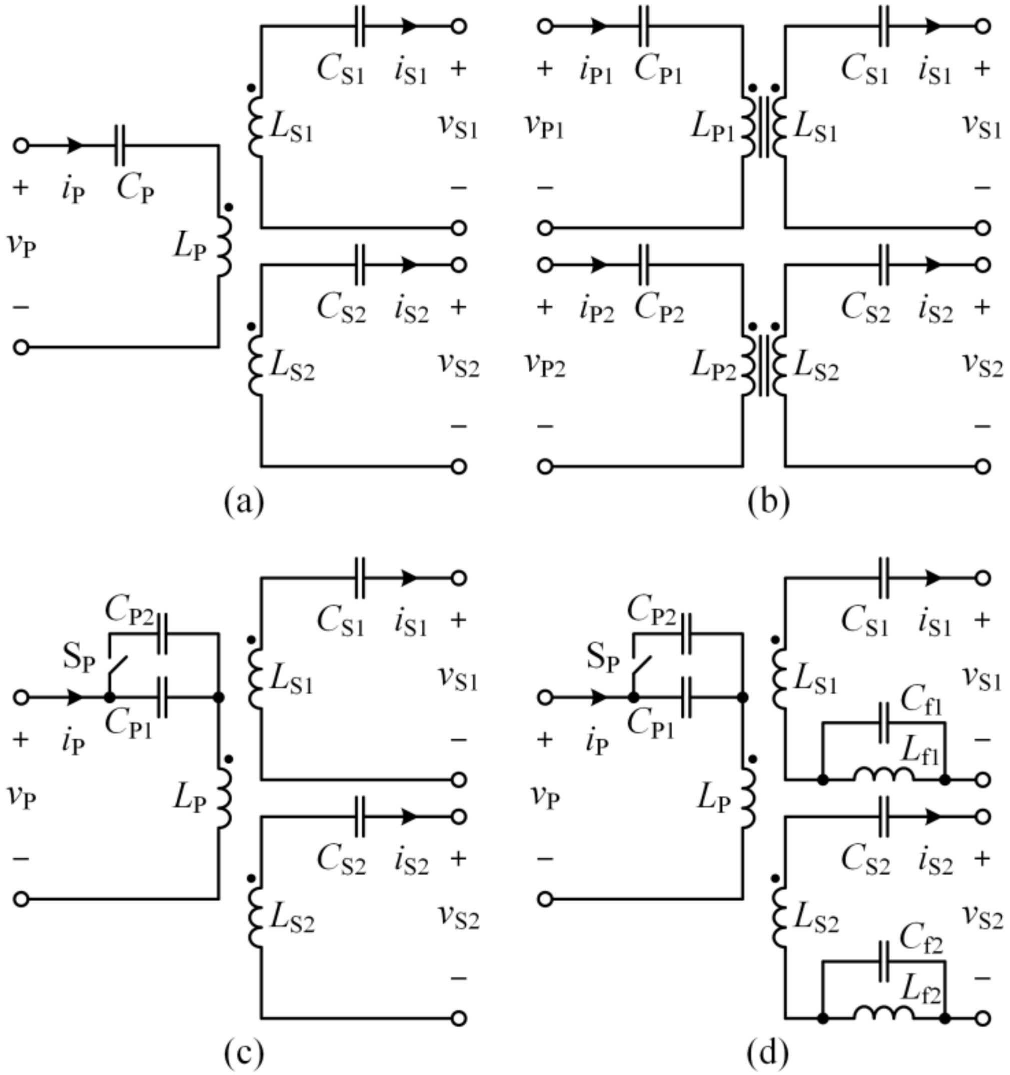

Figure 11. Multi-frequency resonant networks. (**a**) Single primary-side compensation; (**b**) multiple primary-side compensation; (**c**) switched capacitor; (**d**) LC pair to eliminate cross coupling.

Note that the primary side is typically designed to realize power equalization between channels 1 and 2 [49]. Thus, it does not operate at resonant points, i.e., $\omega_1^2 L_P C_P \neq 0$ and $\omega_2^2 L_P C_P \neq 0$. As a result, the system cannot achieve the LIV property and optimal efficiency.

An alternative approach is to use two coils on the primary side [51,120], as shown in Figure 11b. This configuration enables the complete independent design of different channels, i.e.,

$$\begin{cases} \omega_1^2 L_{P1} C_{P1} = \omega_1^2 L_{S1} C_{S1} = 1 \\ \omega_2^2 L_{P2} C_{P2} = \omega_2^2 L_{S2} C_{S2} = 1. \end{cases} \quad (2)$$

The resulted transconductance curves are shown in Figure 12b. It is seen that the LIC property can be achieved. Besides, the coupled current components can be further suppressed.

For the switched capacitor structure, as shown in Figure 11c, the switching frequency needs to satisfy

$$\begin{cases} \omega_1^2 L_{P1} C_{P1} = \omega_1^2 L_{S1} C_{S1} = 1 \\ \omega_2^2 L_{P2} (C_{P1} + C_{P2}) = \omega_2^2 L_{S2} C_{S2} = 1. \end{cases} \quad (3)$$

In this case, the system can achieve comparable performance to that of the multiple primary-side compensation structure.

Notably, the above discussions all ignore the cross coupling between the magnetic couplers. Otherwise, there will also be severe coupling between the outputs of each channel. The cross coupling of the magnetic couplers can be eliminated through both coupler design and circuit design. In terms of coupler design, the basic idea is to use the overlap structure of DD coils and D coils [50]. By canceling out the bipolar and unipolar magnetic fields of the two coils, the cross coupling can be mitigated.

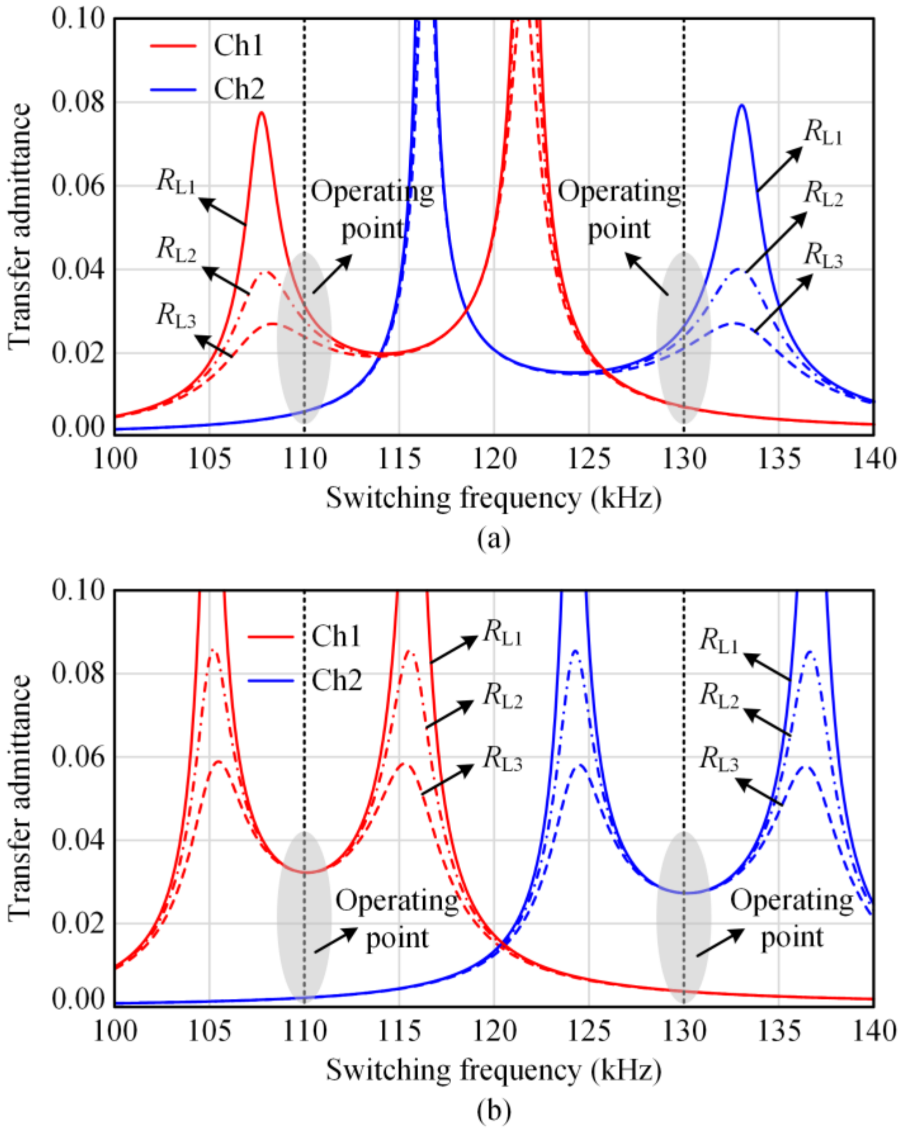

Figure 12. Transconductance of multi-frequency resonant networks. (**a**) Single primary-side compensation. (**b**) multiple primary-side compensation or switched capacitor.

For the circuit design, a commonly used method is to incorporate an LC parallel branch in series with each secondary coil [121,122], as shown in Figure 11d. In channel 1, the LC branch is designed to resonate at f_2, creating an open circuit of f_2 current, namely $\omega_2^2 L_{f1} C_{f1} = 1$. Similarly, in channel 2, the LC branch needs to resonate at f_1 to block f_1 current, i.e., $\omega_1^2 L_{f2} C_{f2} = 1$.

Moreover, the additional LC branch should not affect the circuit's original property. Then we need to design each secondary channel in resonance for all LC components, for example,

$$\begin{cases} j\omega_1 L_{S1} + \dfrac{1}{j\omega_1 C_{S1}} + (j\omega_1 L_{f1} \| \dfrac{1}{j\omega_1 C_{f1}}) = 0 \\ j\omega_2 L_{S2} + \dfrac{1}{j\omega_2 C_{S2}} + (j\omega_2 L_{f2} \| \dfrac{1}{j\omega_2 C_{f2}}) = 0. \end{cases} \quad (4)$$

Based on the above analysis, the multi-coil-based structure substantially increases the number of passive components, such as coupler coils, inductors, and capacitors. As the number of channels increases, the required additional passive components will increase more significantly, particularly due to the extra decoupled LC branches. Therefore, this structure offers limited potential for improving system power density.

4. Matrix Converter-Based Structure

4.1. System Structure

In contrast to multi-coil-based integration, which directly connects motor windings to the IPT converter and employs multiple coils for motor control, matrix converter-based integration merges the rectifier and motor drive into a single unit. As shown in Figure 13, depending on the motor phases, the matrix converters are implemented as either single-phase [41,123–126] or three-phase [27,127–133] structures. Notably, unlike the DC power required for battery charging, the single-phase matrix converter supplies AC power to motor loads.

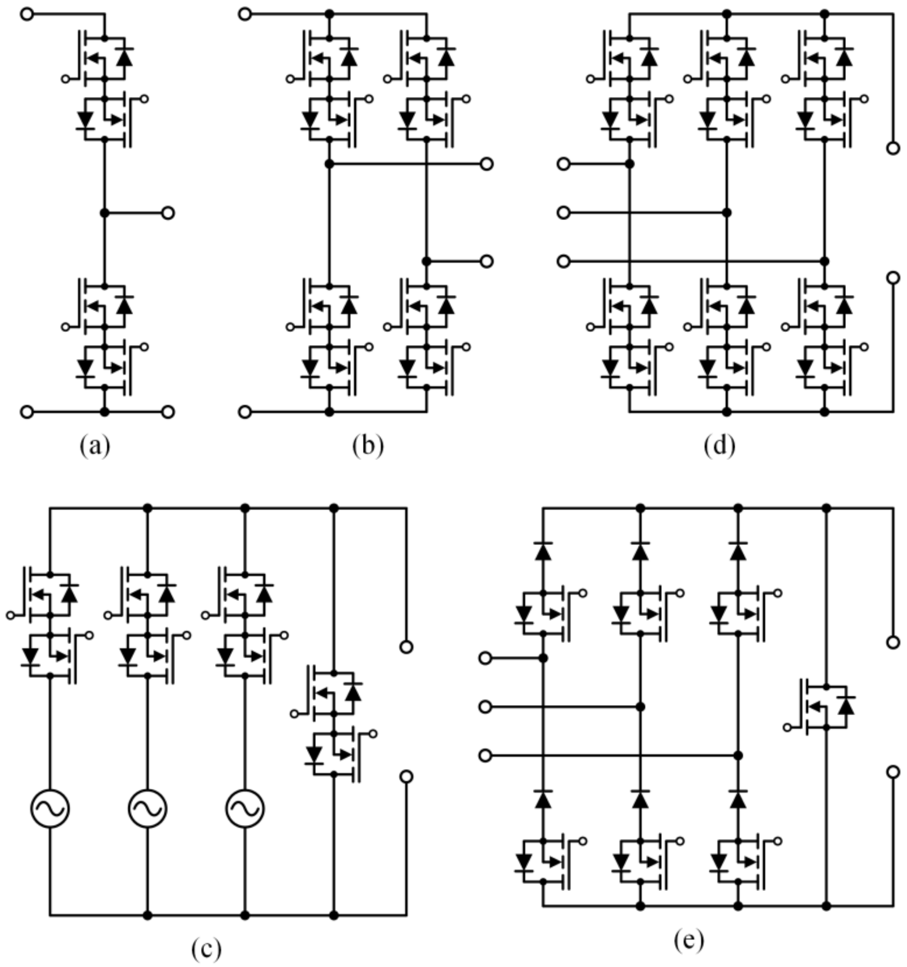

Figure 13. Matrix converters for wireless motor drive systems. (**a**) Single-phase half-bridge structure; (**b**) single-phase full-bridge structure; (**c**) three-phase half-wave structure; (**d**) three-phase bridge structure; (**e**) three-phase simplified bridge structure.

As shown in Figure 13a,b, single-phase matrix converters are further divided into half-bridge [41,123] and full-bridge structures [124–126], respectively. As shown in Figure 13c,d, three-phase matrix converters are primarily implemented in two forms: three-phase half-wave [127,128] and three-phase bridge structures [27,129–132], respectively. The half-wave structure is designed for three-phase four-wire connections, whereas the bridge structure is intended for three-phase three-wire connections. While the bridge structure provides higher voltage utilization and reduced voltage ripple compared to the half-wave structure, it necessitates a greater number of switching devices. As shown in Figure 13e, a simplified structure employing reverse-connected MOSFETs and diodes in place of common-source connected MOSFETs can reduce the number of switching devices [133]. This simplified structure, however, permits only unidirectional current flow and transfers solely positive voltage to the resonant tank. Such constraints increase the susceptibility to over-voltage damage and reduce the system's power capacity. Alternative matrix converters, such as indirect and sparse structures [134,135], are omitted here, as they have not yet been implemented in WPT systems and represent a direction for future research.

Applying matrix converters to wireless motor drive systems facilitates integrated structures that directly convert the high-frequency power from the resonant tank to the low-frequency power required by the motor, and vice versa for grid input. Figure 14a,b illustrate typical matrix converter-based integrated examples for single-phase and three-phase AC motors [27,41], respectively. A higher level of integration can be achieved by also employing a matrix converter on the primary side [28,136], as shown in Figure 14c.

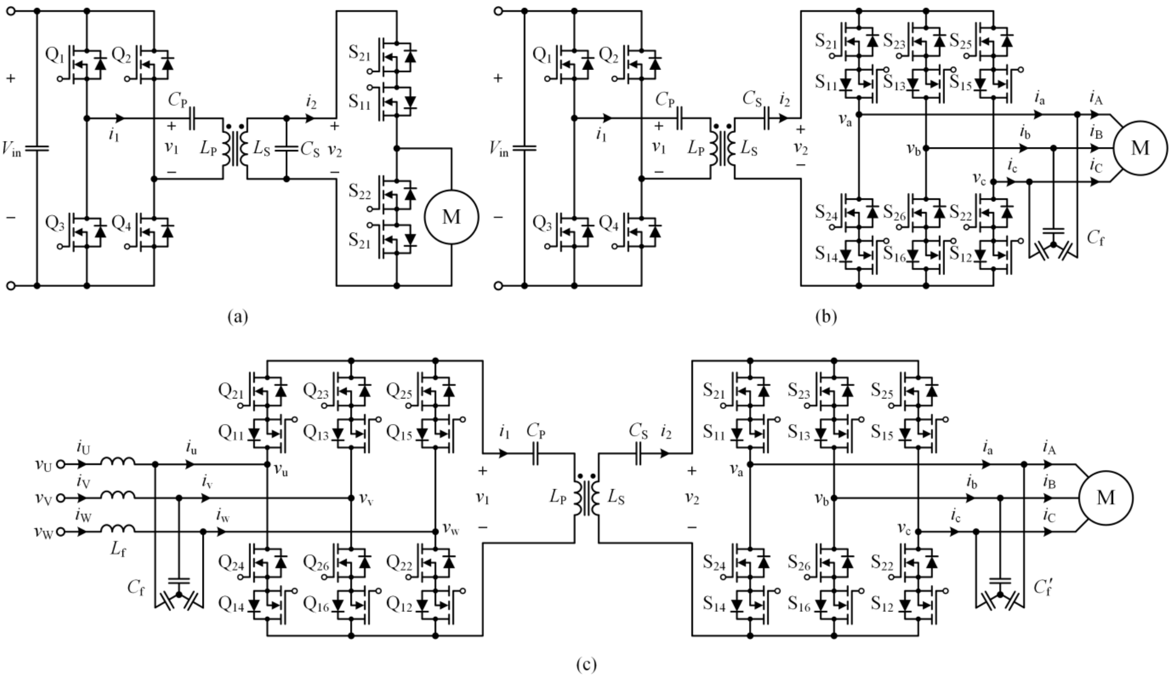

Figure 14. Matrix converter-based integrated wireless motor drive system. (**a**) Single-phase structure; (**b**) three-phase structure; (**c**) dual matrix converter-based structure.

It is worth noting that the required compensation networks depend on the filter type. Consider a single-phase matrix converter on the primary side as an example. In the buck-type configuration shown in Figure 15a, where a capacitor is placed ahead of the matrix converter, a series compensation element (either C_P or L_1) is required after the matrix converter [137]. The structures shown in Figure 14b,c both fall into this category. Alternatively, a boost-type configuration with an inductor placed close to the matrix converter, as shown in Figures 14a or 15b [138], can also be used. In this case, a parallel compensation element (C_P) is required after the matrix converter. As discussed above, parallel compensation is generally avoided in active bridge structures because it necessitates extra inductance and can induce current spikes. Interestingly, boost-type matrix converter-based WMD systems offer a promising application for the parallel compensation topologies.

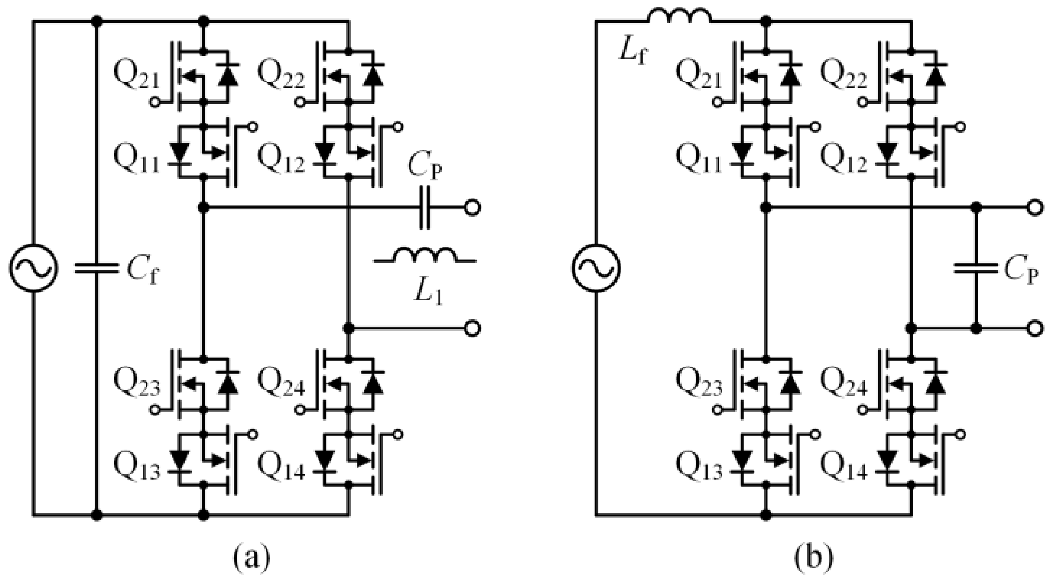

Figure 15. Compensation networks for matrix converter-based integrated wireless motor drive system. (**a**) Series compensation; (**b**) parallel compensation.

4.2. System Operation

The matrix converter-based integrated wireless motor drive system primarily operates with the pulse density modulation (PDM) [39,40,123,126,133] and the space vector modulation (SVM) [27,28,129–132]. In PDM, the system alternates between energy injection and free oscillation modes. Output power is regulated by adjusting the number of switching pulses to control the energy injected into the resonant tank. This method offers the advantages of zero current switching (ZCS) and reduced switching times. Nevertheless, conventional PDM focuses solely on output regulation and neglects the total harmonic distortion (THD) of the grid or motor current. An improved approach to address this limitation is the use of delta-sigma modulation [39,40].

The diagram of delta-sigma modulation is shown in Figure 16a, using the grid-side application as an illustrative example. The reference signals ($v_{ref\_u,v,w}$) share the same envelope as the grid input. The differences (delta signals, $\Delta_{u,v,w}$) between reference signals and comparator feedback signals ($v'_{co\_u,v,w}$) are integrated to produce the sigma signals ($\Sigma_{u,v,w}$). By comparing the sigma signals against threshold values and cross-comparing them among phases, the pulse signals ($v_{co\_u,v,w}$) can be generated. These pulses are then converted into gate drive signals through logic processing. As shown in Figure 16b, the fundamental principle of delta sigma modulation is to vary the pulse density to track the reference envelope: higher reference amplitudes produce higher pulse densities, and vice versa. This characteristic enables superior THD performance compared to conventional methods. Furthermore, the overall pulse density is determined by the modulation index, ensuring that the output power remains controllable.

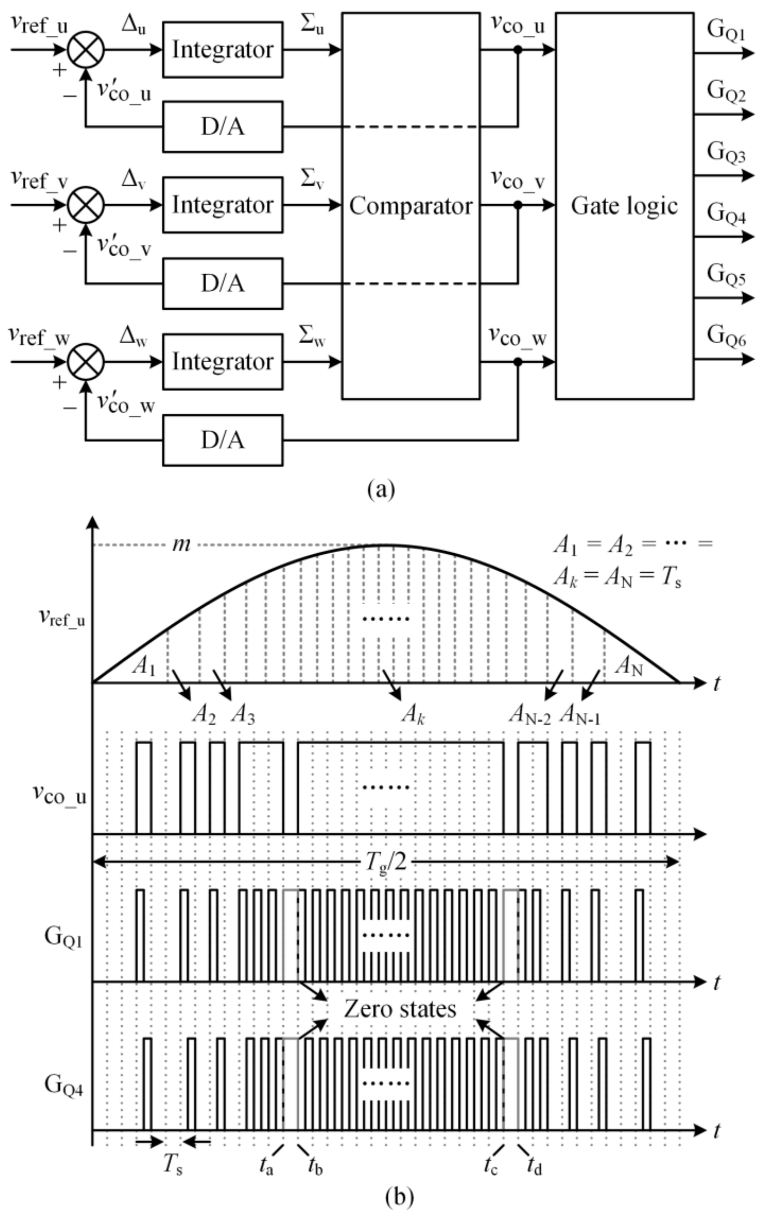

Figure 16. Delta-sigma modulation. (**a**) Diagram; (**b**) operating principle.

Besides pulse density modulation, pulse width modulation offers an alternative method for the matrix converter-based wireless motor drive system. The phase shift method, for instance, has been investigated for this purpose [124,128]. However, like conventional PDM, this method offers only output control and usually results in poor THD. Consequently, SVM is the more widely adopted solution.

The SVM technique of the matrix converter is similar to that of the CSI motor drive [106], with both employing a six-sector period. A key distinction lies in the reference vector direction. As shown in Figure 17a, the CSI motor drive operates with a DC current and uses a single set of basic vectors shown in Figure 18a. In contrast, as shown in Figure 17b, the matrix converter handles an AC resonant current and therefore requires two complementary sets of basic vectors—one for the positive half-cycle and another for the negative half-cycle, corresponding to Figure 18a,b, respectively.

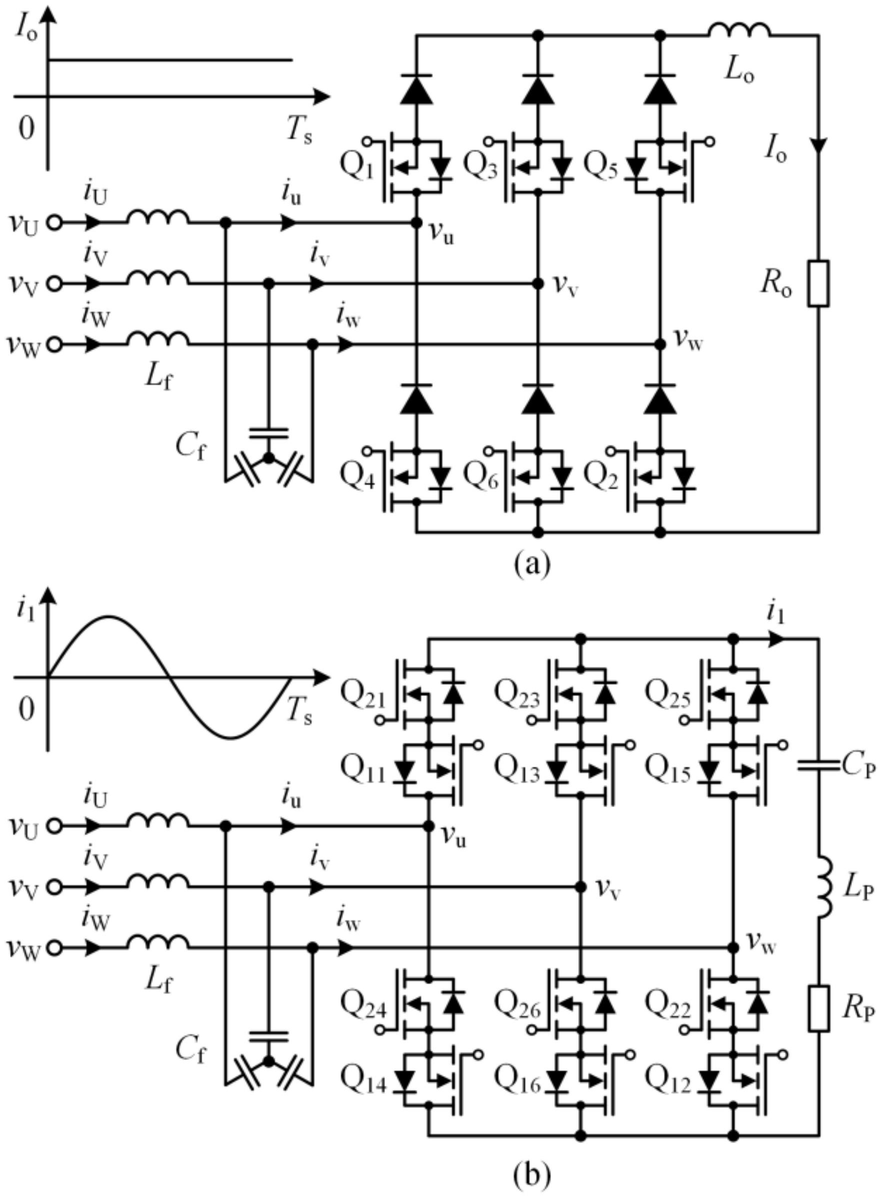

Figure 17. Comparison between CSI and matrix converter-based system. (**a**) CSI; (**b**) matrix converter-based system.

A further distinction from the conventional CSI drive is that, in the matrix converter-based system, the AC reference vectors exhibit a phase shift between the resonant voltage and current. Moreover, the time-varying amplitude of these AC vectors within a switching period requires a modified dwell time calculation approach.

The phase shift effect in matrix converter-based wireless motor drives is fundamentally caused by reactive power in the resonant tank [131]. As shown in Figure 19a, conventional half-wave symmetric waveforms fail to cancel reactive power components Q_{12} and Q_{45}. To solve this problem, the period-flip method shown in Figure 19b inverts the waveforms in alternating switching periods [131], allowing reactive power components Q_{12} and Q_{67} to cancel out. Then the phase shift effect caused by component tolerance, load variation, and misalignment can be mitigated. Other techniques, such as using antisymmetric waveforms [28,132], operate on the same principle and provide similar benefits.

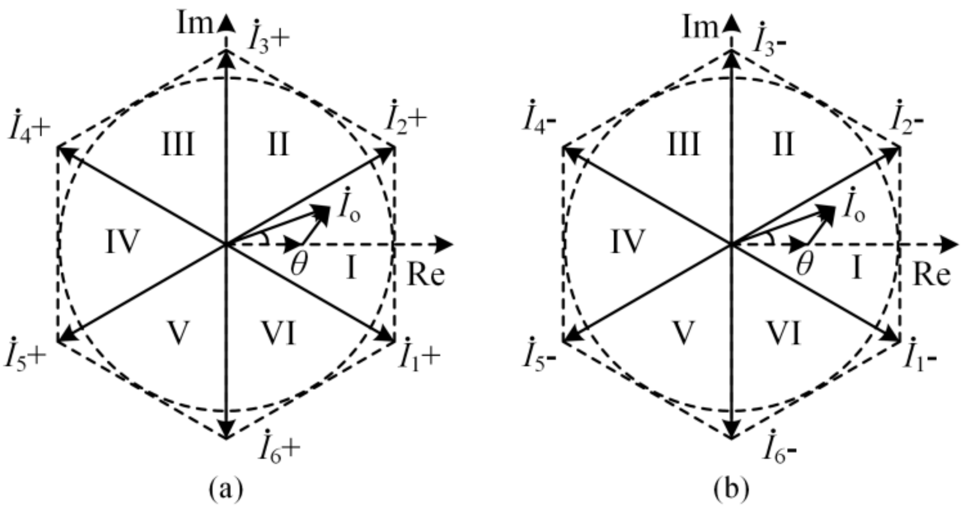

Figure 18. Modulation vectors. (**a**) Positive vectors; (**b**) negative vectors.

The other challenge is calculating dwell time. For the system shown in Figure 17 under consideration, the dwell time of basic vectors during a switching period is

$$\begin{cases} T_1 = \dfrac{I_g}{i_1} T_s \cos\left[\theta - \dfrac{\pi}{3}(N-2)\right] \\ T_2 = \dfrac{I_g}{i_1} T_s \cos\left(\theta - \dfrac{\pi}{3}N\right) \\ T_0 = T_s - T_1 - T_2. \end{cases} \tag{5}$$

where I_g is the synthesized current, i_1 is the converter output current, and N is the fan sector. For the CSI motor drive, the dwell time is obtained by substituting I_o for i_1 in (5). As I_o is stable in the CSI motor drive, the resulting synthesized waveform normally yields good THD performance. In the matrix converter, however, the continuous variation of i_1 throughout the switching period makes precise real-time determination of dwell time difficult. A common practice is to approximate i_1 with its RMS or peak value for calculation [27]. However, this approximation introduces significant errors, resulting in substantial harmonics in the grid or motor winding current.

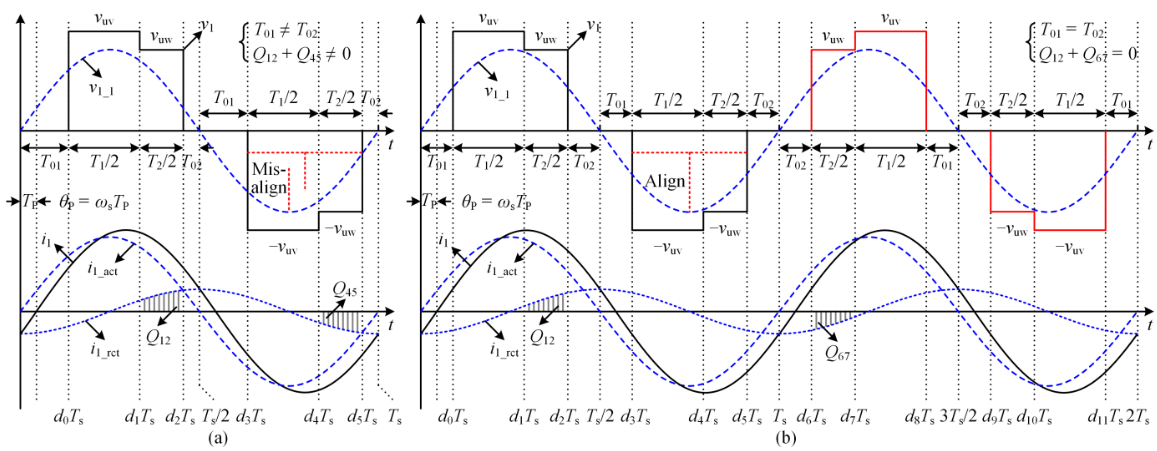

Figure 19. SVM waveforms. (**a**) half-wave symmetric waveforms; (**b**) period flip waveforms.

To improve the precision of the dwell time calculation, the area equivalent principle is also applied to SVM in each switching period. Referring to the denotation in Figure 19, the dwell time relationship of the matrix converter-based system can be obtained as

$$\begin{cases}\cos(\omega_s d_1 T_s) - \cos(\omega_s d_0 T_s) = 2m\cos(\theta - 2\pi/3) \\ \cos(\omega_s d_2 T_s) - \cos(\omega_s d_1 T_s) = 2m\cos(\theta + 2\pi/3).\end{cases} \tag{6}$$

For the half-wave symmetric modulation, it lacks an additional equation to solve d_0, d_1, and d_2, so approximation methods [131,132] are usually required. For the periodic flip or antisymmetric modulation, the relationship $T_{01} = T_{02}$ is satisfied [28], so the accurate expression of the dwell time can be obtained.

5. Discussion and Future Perspective

5.1. Discussion

Table 6 presents a comparison of various wireless motor drive structures. When comparing multi-coil-based integrated structures with matrix converter-based structures, it is evident that multi-coil-based structures are easier to implement and offer better robustness due to the extensive use of passive components. However, this advantage comes at the cost of larger size and weight. Besides, the multi-coil configuration restricts bidirectional power flow in the system. Moreover, misalignment will exacerbate the cross-coupling and power imbalance problems. Therefore, multi-coil-based structures exhibit poor tolerance to misalignment.

Due to semiconductor device limitations, matrix converter-based structures are more fragile than multi-coil-based structures. The increased use of switching devices also complicates the control and modulation strategies of matrix converter-based structures. Besides, since there are no electrolytic capacitors on the motor side, misalignment can directly affect the motor's performance, leading to poor misalignment tolerance. Nevertheless, this structure enables easy realization of bidirectional power flow and allows for significant reductions in system volume and weight. In fact, the concept of using semiconductor devices to replace passive components has been popular in power electronics. In addition to matrix converters, the active capacitor [139,140] and the solid-state transformer [141,142] have also drawn growing attention. Given the development trend, conducting further research on matrix converter-based integrated structures remains highly justified.

Compared to the integrated structure, the cascaded structure offers greater compatibility with different motors and improved misalignment tolerance due to the decoupled filter components. Moreover, the cascaded structure allows for direct application of conventional motor control methods, resulting in better motor performance than integrated structures. However, it is noted that the multi-stage power conversion will introduce extra losses, and the bulk decoupled filters will impact the system's power density. Based on existing research and issues, some future research perspectives are outlined below.

Table 6. Cascaded and Integrated Structures.

Structure	Cascaded [13–22,46,47]	Multi-Coil [25,26,33–36,48–54]	Matrix Converter [27,28,39–41]
Bidirectional power flow	Yes	No	Yes
Misalignment tolerance	Good	Bad	Bad
Motor performance	Good	Bad	Bad
Robustness	Medium	High	Low
Volume	Medium	Large	Small
Challenges	• Low power density • Multi-stage power conversion • Wireless communication	• Low power density • Unidirectional power flow • Poor misalignment tolerance • Limited motor compatibility • Wireless communication	• Low reliability • Complex control and modulation • Poor misalignment tolerance • Wireless communication

5.2. Future Perspective

5.2.1. Cascaded Wireless Motor Drive System Based on the CSI Configuration

As discussed above, the WPT converter can be categorized as either LIV or LIC types. Meanwhile, the motor drive can adopt either VSI or CSI configurations. Then, we obtain four possible configurations: LIV/VSI, LIV/CSI, LIC/VSI, and LIC/CSI. While existing research has explored the LIV/VSI and LIC/VSI structures, the performance of the LIV/CSI and LIC/CSI structures remains unexamined. Therefore, it is necessary to conduct an in-depth study of both LIC/VSI and LIC/CSI structures. Furthermore, a comprehensive comparison among all four cascaded configurations would provide valuable guidance for topology selection in practical applications.

5.2.2. Bidirectional Power Flow for the Wireless Motor Drive System

Previous studies have primarily focused on unidirectional power flow from the power source to the motor. However, bidirectional power flow is essential for braking energy recovery. In multi-coil-based structures, the presence of diode bridges and cross-coupling between the coupler coils makes it challenging to realize bidirectional power flow.

In contrast, for cascaded structures employing LIC compensation topologies, such as S/S and LCC/LCC, which are typically symmetric, bidirectional power flow is easier to achieve. However, the CSI motor drive has to be replaced with a matrix converter. As an active rectifier also has to be used on the secondary side, the system cost will increase significantly. Conversely, LIV compensation topologies, such as S/P and LCC/S, are generally asymmetric, complicating the bidirectional flow control. Therefore, either an optimized circuit configuration or a bidirectional power control strategy is essential for the cascaded wireless motor drive system.

For matrix converter-based wireless motor drive systems, the symmetric configuration makes them particularly suitable for bidirectional power flow applications. Nevertheless, the lack of effective modulation strategies remains a limitation for the further development of this structure.

5.2.3. Advanced Modulation Strategy for the Matrix Converter-Based Wireless Motor Drive System

Delta-sigma modulation and SVM strategies have been studied for the matrix converter-based wireless motor drive system [28,39,40,131,132]. While the delta-sigma modulation offers reduced switching times and device stresses, no effective method has been proposed to eliminate the phase shift effect on the THD performance. The improved SVM can mitigate phase shift effects and achieve better THD results, but it results in higher switching stresses. Besides, both modulation strategies are highly dependent on the waveform quality of the resonant current. For example, a significant increase in harmonics within the resonant tank can lead to severely poor THD results on the low-frequency AC side. Moreover, the effects of misalignment and wireless communication have not been addressed in existing studies. In view of these limitations, modulation strategies should also be further improved for the matrix converter-based wireless motor drive system.

Besides, implementing motor control and modulation requires high computational ability. Reducing computational complexity while maintaining high control performance remains an important research direction. Therefore, implementing advanced control and modulation algorithms on practical hardware platforms, such as digital signal processors (DSPs), field-programmable gate arrays (FPGAs), and other embedded controllers, requires further investigation to ensure sufficient processing capability and real-time execution.

5.2.4. Wireless Integrated Modular Motor Drive (IMMD)

Following circuit-level integration, mechanical-level integration should be considered. Similar to conventional IMMD systems [143,144], where the motor, control unit, communication module, and protection circuits are combined into a single compact package, the wireless IMMD system also integrates the motor and its associated electronics. This configuration significantly reduces the overall system size by enabling shared cooling between the motor and drive.

However, housing both the motor and drive within a single enclosure introduces several technical challenges. For example, the power electronics must be carefully designed to withstand the harsh thermal and vibrational conditions generated by the motor’s operation. Consequently, thermal management becomes a critical consideration in IMMD systems.

Furthermore, the receiver coils typically operate at high frequencies (e.g., 85 kHz or higher), while the motor windings operate at much lower frequencies (e.g., 50 Hz or a few hundred Hz). This substantial frequency disparity complicates both magnetic and EMI design.

5.2.5. Simultaneous Wireless Power and Signal Transmission

Commercial wireless communication modules such as Bluetooth, Wi-Fi, and Zigbee are commonly used in wireless power transfer systems. However, these modules introduce variable delays on the order of milliseconds [145]. In contrast, motor drive systems typically employ optocouplers, transformers, or capacitive isolators, which achieve much lower delays with microsecond timescales. Given that motor dynamics respond in a millisecond timescale, the latency introduced by commercial wireless modules is unsuitable for real-time control in wireless motor drive systems.

Consequently, simultaneous wireless power and signal transfer methods have been developed [145,146]. These methods transmit signals either by modulating the power channel or by incorporating additional coils. By enabling real-time communication and reducing device pairing time, simultaneous wireless power and signal transfer methods offer significantly lower latency compared to traditional wireless solutions.

However, there still exist several challenges. First, the additional coils or modulation circuits increase system complexity and volume. This poses a particular difficulty for wireless motor drive applications, where high power density is critical due to the limited space within motor chambers. Second, the proximity of power and signal components leads to significant EMI challenges. Furthermore, signal coils are typically much smaller than power coils, making them more susceptible to misalignment effects that can degrade communication performance.

Therefore, there remains a pressing need for compact and reliable wireless communication solutions specifically optimized for wireless motor drive systems.

5.2.6. Artificial Intelligence-Assisted Motor Control for Wireless Motor Drive Systems

Future WMD systems will face more control challenges from nonlinear characteristics, parameter variations, coupler misalignment, and dynamic operating conditions. Although conventional control methods have demonstrated satisfactory performance under well-defined conditions, their adaptability to uncertain environments remains limited. Fortunately, artificial intelligence (AI)-based techniques provide a promising approach for future motor controllers [147]. AI algorithms, such as neural networks and reinforcement learning, can be integrated into conventional control frameworks to optimize controller parameters, compensate for nonlinear disturbances, and enhance motor trajectory tracking performance under varying operating conditions.

Despite the advantages, the practical implementation of AI-based motor control remains challenging due to hardware constraints, data requirements, and real-time execution limitations. Therefore, future research should focus on hardware-oriented AI implementation, such as FPGA-based controllers and dedicated AI accelerator integration. Moreover, edge computing can be employed to enable local data processing and model inference, thereby reducing communication latency and improving system responsiveness. Developing lightweight, reliable, and real-time AI solutions is essential for realizing intelligent WMD systems with high performance and practical applicability.

6. Conclusions

The paper provides a critical review of wireless motor drive systems, focusing on three typical structures: the cascaded structure, the multi-coil-based structure, and the matrix converter-based structure. For the cascaded structure, four possible configurations, LIV/CSI, LIV/VSI, LIC/CSI, and LIC/VSI, are analyzed and compared. Future research should place greater emphasis on CSI-based cascaded structures and bidirectional power flow. The paper then explores the multi-coil-based and matrix converter-based structures within the integrated configuration. It concludes that multi-coil-based structures offer higher robustness while matrix converter-based structures enable higher power density. Multiple frequency control is essential for the multi-coil-based structure. Different motor windings are assigned distinct resonant-frequency channels to realize independent control. However, the extensive use of coupler coils and decoupling branches limits the practicality of multi-coil-based structures. For the matrix converter-based structure, modulation strategies are highlighted as a central challenge. Although existing research has made improvements to the modulation strategy, many practical factors, such as component stresses, misalignment effects, and wireless communication latency, remain unaddressed. Finally, the paper provides a comparative summary of the three structures and offers future perspectives based on the current state of research.

7. Biographies of the Authors

Xin Felix Chen received the B.S. and M.S. degrees in electrical engineering from Nanjing University of Aeronautics and Astronautics, Nanjing, China, in 2016 and 2019, respectively, and the Ph.D. degree in electrical engineering from City University of Hong Kong, Hong Kong, China, in 2025. His research interests include wireless motor drives and resonant converters.

Yangbin Zeng received the B.Sc. degree in building electrical and intelligent from Xiangtan University, Xiangtan, China, in 2015, and the Ph.D. degree in electrical engineering from Beijing Jiaotong University, Beijing, China, in 2021. From 2021 to 2024, he was a Post-Doctoral Researcher at the Department of Electrical Engineering, Tsinghua University, Beijing, China. From 2023 to 2024, he was a Post-Doctoral Researcher at the City University of Hong Kong, Hong Kong, China. He is currently an Associate Professor with the School of Electric Power, South China University of Technology, Guangzhou, China. His current research interests include real-time simulation, power router, and soft-switching techniques.

Chi K. Tse (Fellow, IEEE) received the B.Eng. (first class Hons.) and the Ph.D. degree in electrical engineering from the University of Melbourne, Melbourne, Australia, in 1987 and 1991, respectively.

Currently, he is an Associate Vice President of Innovation, Director of Academy of Innovation, and Chair Professor of Electrical Engineering with City University of Hong Kong, Hong Kong, China. His research interests include power electronics, nonlinear systems, and complex network applications.

Dr. Tse was the recipient of a number of research and invention prizes including the IEEE CASS Charles A. Desoer Technical Achievement Award, in 2022 and a few Best Paper Prizes from IEEE and other journals, as well as Gold Medal with Jury's Commendations and Grand Prizes in International Exhibition of Inventions of Geneva 2024, Asia Exhibition of Innovations and Inventions 2023, and Silicon Valley International Invention Festival 2019. He has been appointed to honorary professorship and distinguished fellowship by a few Australian, Canadian, and Chinese universities, including Chang Jiang Scholar Chair Professor with Huazhong University of Science and Technology, Honorary Professor of Melbourne University, Melbourne, Australia, and Distinguished Professor-at-Large with the University of Western Australia. He also served as the Panel Member of Hong Kong Research Grants Council, and member of several professional and government committees. In 2005, 2010, and 2018, he was selected as an IEEE Distinguished Lecturer. In 2006, he chaired the IEEE CAS Technical Committee on Nonlinear Circuits and Systems. He serves and has served as the Editor-in-Chief of IEEE TRANSACTIONS ON CIRCUITS AND SYSTEMS II, from 2016 to 2019; IEEE CIRCUITS AND SYSTEMS MAGAZINE, from 2013 to 2016; IEICE Nonlinear Theory and Applications, since 2013; an Associate Editor of a few other IEEE journals; and on the Editorial Board of IEEE PROCEEDINGS, from 2021 to 2024. He has served on a number of IEEE committees including the IEEE Fellows Committee and the IEEE Awards Committee, and chaired the Steering Committee of the IEEE TRANSACTIONS ON NETWORK SCIENCE AND ENGINEERING.

C. Q. Jiang received the B.Eng. and M.Eng. degrees (first class Hons.) in electrical engineering and automation from Wuhan University, Wuhan, China, in 2012 and 2015, respectively, and the Ph.D. degree in electrical and electronic engineering from The University of Hong Kong, Hong Kong, China, in 2019.

Currently, he is an Associate Professor with the Department of Electrical Engineering, a Faculty Member with the State Key Laboratory of Terahertz and Millimeter Waves, City University of Hong Kong, Hong Kong SAR, China. From 2019 to 2021, he was a Postdoctoral Research Associate with the University of Cambridge, Cambridge, U.K. Since 2021, he has been affiliated with Clare Hall, University of Cambridge, Cambridge, U.K. In 2019, he was a Visiting Researcher with Nanyang Technological University, Singapore. His research interests include power electronics, wireless power transfer, electric machines and drives, and electric vehicle (EV) technologies.

Dr. Jiang was the recipient of Y-LOT's Hong Kong SciTech Pioneers Award, Gold Medal with the Silicon Valley International Invention Festival, Gold Medals with Congratulations of the Jury in International Exhibition of Inventions of Geneva, Winner of CAPE Acorn Blue Sky Research Award at the University of Cambridge, Cambridge, U.K., and Gold Medal in 3rd Asia Exhibition of Innovations and Inventions. Currently, he is an Associate Editor of IET Renewable Power Generation, and a Guest Editor of IEEE OPEN JOURNAL OF VEHICULAR TECHNOLOGY and IEEE TRANSACTIONS ON POWER ELECTRONICS LETTERS.

Qianhong Chen received the B.S., M.S. and Ph.D. degrees in electrical engineering from Nanjing University of Aeronautics and Astronautics (NUAA), Nanjing, China, in 1995, 1998 and 2001, respectively. Currently, she is a Professor with the Department of Electrical Engineering, NUAA. Her research interests include application of integrated-magnetics, wireless power transfer and high power density power converters.

Ching-Ming Lai received the Ph.D. degree in electrical engineering from the National Tsing Hua University, Taipei, Taiwan, in 2010.

From 2009 to 2012, he was a Senior Research and Development Engineer with Lite-On Technology Corporation, Taipei, Taiwan. From 2014 to 2019, he was a Faculty Member with the Department of Vehicle Engineering, National Taipei University of Technology (Taipei Tech), Taipei, Taiwan. Since 2019, he has been with the Department of Electrical Engineering, National Chung Hsing University (NCHU), Taichung, Taiwan. Currently, he is a Professor and the Director of the Intelligent Electric Vehicle and Green Energy Center, NCHU. His research interests include system integration, electric vehicles, power electronics, green energy technologies, and intelligent transportation.

Dr. Lai was the recipient of the 2008 Young Authors Award for Practical Application from the Society of Instrument and Control Engineers, Japan, Best Paper Award at the 2013 IEEE International Conference on Power Electronics and Drive Systems, Technical Award Paper of 2024 IEEE International Conference on Power Electronics Systems and Applications. He received Dr. Shechtman Youth Researcher Award from Taipei Tech, in 2018, Outstanding Youth Engineer Award from Chinese Institute of Engineers-Taichung Chapter, in 2020, and the Outstanding Engineering Professor from Chinese Institute of Engineers-Taichung Chapter, in 2024. In addition, according to Elsevier, since 2021, he has been listed in the World's Top 2% of Scientists (Field: Energy). Since 2024, he serves as the Founder and Chair of the IEEE Systems Council Taipei Chapter. Besides, he serviced as the TPC Vice Chair of IEEE ECCE Asia-2025, General Chair of IEEE RASSE-2024, the Co-Chair of IEEE IFEEC-2021, the Tutorial Chair of IEEE IFEEC-2021, IEEEWiPDA-2019, and IEEE IFEEC-2015. Since 2017, he has been the Editor of IEEE TRANSACTIONS ON VEHICULAR TECHNOLOGY; and an Associate Editor of IEEE ACCESS, since 2021 and IEEE SYSTEMS JOURNAL, since 2025.

Author Contributions

X.F.C.: investigation, writing—original draft preparation; Y.Z.: writing—original draft preparation; C.K.T.: supervision, writing—reviewing and editing; C.Q.J.: writing—reviewing and editing; Q.C.: writing—reviewing and editing; C.-M.L.: writing—reviewing and editing. All authors have read and agreed to the published version of the manuscript.

Funding

This research was funded by Hong Kong RGC Theme-Based Research Scheme Project T23-701/20R and Hong Kong RGC GRF 112052/22E.

Institutional Review Board Statement

Not applicable.

Informed Consent Statement

Not applicable.

Data Availability Statement

The data that support the findings of this study are available from the corresponding author upon reasonable request. The authors ensure that the data will be retained for at least 10 years after publication in compliance with the journal's policy.

Conflicts of Interest

The authors declare no conflict of interest.

Use of AI and AI-Assisted Technologies

No AI tools were utilized for this paper.

References

1. Bosshard, R.; Kolar, J.W. Multi-Objective Optimization of 50 kW/85 kHz IPT System for Public Transport. *IEEE J. Emerg. Sel. Top. Power Electron.* **2016**, *4*, 1370–1382.
2. Ahmad, A.; Alam, M.S.; Chabaan, R. A Comprehensive Review of Wireless Charging Technologies for Electric Vehicles. *IEEE Trans. Transp. Electrif.* **2018**, *4*, 38–63.
3. Bagchi, A.C.; Kamineni, A.; Zane, R.A.; et al. Review and Comparative Analysis of Topologies and Control Methods in Dynamic Wireless Charging of Electric Vehicles. *IEEE J. Emerg. Sel. Top. Power Electron.* **2021**, *9*, 4947–4962.
4. Chen, Q.; Wong, S.C.; Tse, C.K.; et al. Analysis, Design, and Control of a Transcutaneous Power Regulator for Artificial Hearts. *IEEE Trans. Biomed. Circuits Syst.* **2009**, *3*, 23–31.
5. Knecht, O.; Kolar, J.W. Performance Evaluation of Series-Compensated IPT Systems for Transcutaneous Energy Transfer. *IEEE Trans. Power Electron.* **2019**, *34*, 438–451.
6. Roy, S.; Azad, A.N.M.W.; Baidya, S.; et al. Powering Solutions for Biomedical Sensors and Implants Inside the Human Body: A Comprehensive Review on Energy Harvesting Units, Energy Storage, and Wireless Power Transfer Techniques. *IEEE Trans. Power Electron.* **2022**, *37*, 12237–12263.
7. Jang, Y.; Jovanovic, M.M. A Contactless Electrical Energy Transmission System for Portable-Telephone Battery Chargers. *IEEE Trans. Ind. Electron.* **2003**, *50*, 520–527.
8. Hui, S.Y.R.; Ho, W.C. A New Generation of Universal Contactless Battery Charging Platform for Portable Consumer Electronic Equipment. *IEEE Trans. Power Electron.* **2005**, *20*, 620–627.
9. Hui, S.Y.R.; Zhong, W.; Lee, C.K. A Critical Review of Recent Progress in Mid-Range Wireless Power Transfer. *IEEE Trans. Power Electron.* **2014**, *29*, 4500–4511.
10. Kikuchi, S.; Sakata, T.; Takahashi, E.; et al. Development of Wireless Power Transfer System for Robot Arm with Rotary and Linear Movement. In Proceedings of the 2016 IEEE International Conference on Advanced Intelligent Mechatronics (AIM), Banff, AB, Canada, 12–15 July 2016; pp. 1616–1621.
11. Zhang, C.; Lin, D.; Hui, S.Y.R. Ball-Joint Wireless Power Transfer Systems. *IEEE Trans. Power Electron.* **2018**, *33*, 65–72.
12. Matsumoto, H.; Shibako, Y.; Neba, Y. Contactless Power Transfer System for AGVs. *IEEE Trans. Ind. Electron.* **2018**, *65*, 251–260.

13. Gunji, D.; Imura, T.; Fujimoto, H. Stability Analysis of Constant Power Load and Load Voltage Control Method for Wireless In-Wheel Motor. In Proceedings of the IEEE 9th International Conference on Power Electronics (ECCE Asia), Seoul, Korea, 1–5 June 2015; pp. 1944–1949.
14. Sato, M.; Yamamoto, G.; Gunji, D.; et al. Development of Wireless In-Wheel Motor Using Magnetic Resonance Coupling. *IEEE Trans. Power Electron.* **2016**, *31*, 5270–5278.
15. Sato, M.; Guidi, G.; Imura, T.; et al. Model for Loss Calculation of Wireless In-Wheel Motor Concept Based on Magnetic Resonant Coupling. In Proceedings of the IEEE 17th Workshop on Control and Modeling for Power Electronics, Trondheim, Norway, 27–30 June 2016; pp. 1–6.
16. Fujimoto, H.; Shimizu, O.; Nagai, S.; et al. Development of Wireless In-Wheel Motors for Dynamic Charging: From 2nd to 3rd Generation. In Proceedings of the IEEE PELS Workshop on Emerging Technologies: Wireless Power Transfer, Seoul, Korea, 15–19 November 2020; pp. 56–61.
17. Chen, X.F.; Tse, C.K.; Jiang, C.Q.; et al. Soft Switching Based Design of Wireless In-Wheel Motor Drive System with Series-Capacitor-Parallel Compensation. *IEEE J. Emerg. Sel. Top. Ind. Electron.* **2026**, *14*, 2655–2667.
18. Chen, Y.; Gan, C.; Shi, H.; et al. Auxiliary-Circuit-Free Maximum Power Efficiency Tracking Scheme for Wireless Motor System with Source-Load Coupling. *IEEE Trans. Ind. Electron.* **2023**, *70*, 3414–3425.
19. Chen, Y.; Gan, C.; Shi, H.; et al. DC-Link Voltage Control for Series-Parallel Wireless Motor without Communication Considering System Nonlinearity. In Proceedings of the IEEE 21st International Conference on Electrical Machines and Systems, Zhuhai, China, 5–8 November 2023; pp. 485–490.
20. Chen, Y.; Gan, C.; Shi, H.; et al. Active Power Allocation Strategy for a Novel Wireless Open-Winding Motor System with Improved Antimisalignment Capability. *IEEE Trans. Ind. Electron.* **2023**, *70*, 12071–12081.
21. Chen, Y.; Gan, C.; Shi, H.; et al. Efficiency Optimization and Resilience Improvement in Wireless Motor System with Flexible DC-Link Voltage Regulation. *IEEE Trans. Energy Convers.* **2023**, *38*, 1803–1814.
22. Chen, S.; Ding, W.; Huo, L.; et al. Design of Double-LCC-Compensated Wireless PMSM System with Variable DC-Link Voltage Considering Efficiency Optimization and Dynamic Improvement. *IEEE Trans. Power Electron.* **2024**, *39*, 3186–3199.
23. Dong, S.; Chen, Y.; Chen, X.; et al. Modeling and Stability Enhancement Method of Wireless Motor System Based on Damping Reconstruction Control. *IEEE Trans. Power Electron.* **2024**, *39*, 10651–10664.
24. Jin, P.; Wang, H.; Xu, H.; et al. Stability Analysis for Three-Stage Serial PMSM Drive System Based on Bidirectional WPT. *IEEE Trans. Ind. Electron.* **2025**, *72*, 4526–4534.
25. Huang, Y.; Gao, X.; Song, Z.; et al. A Novel Wireless Motor Based on Three-Phase Six-Stator-Winding PMSM. *IEEE Trans. Ind. Electron.* **2024**, *71*, 7590–7598.
26. Liu, Y.; Wang, W.; Liu, S.; et al. A Compact Wireless Permanent Magnet Synchronous Motor System with Precise Speed and Position Control. *IEEE Trans. Ind. Electron.* **2024**, *71*, 11852–11863.
27. Li, C.; Wang, Z.; Xu, Y. A Wireless-Power-Transfer-Based Three-Phase PMSM Drive System with Matrix Converter. *IEEE Trans. Ind. Electron.* **2023**, *70*, 2307–2317.
28. Chen, X.F.; Tse, C.K.; Jiang, C.Q.; et al. Dual Matrix Converter Based Wireless Power Transfer System. *IEEE Trans. Power Electron.* **2025**, *40*, 18474–18488.
29. Kim, J.H.; Lee, B.S.; Lee, J.H.; et al. Development of 1-MW Inductive Power Transfer System for a High-Speed Train. *IEEE Trans. Ind. Electron.* **2015**, *62*, 6242–6250.
30. Xue, Z.; Chau, K.T.; Liu, W.; et al. Magnetic-Free Wireless Self-Direct Drive Motor System for Biomedical Applications with High-Robustness. *IEEE Trans. Power Electron.* **2024**, *39*, 2882–2891.
31. Liu, W.; Chau, K.T.; Lee, C.H.T.; et al. Wireless Power and Drive Transfer for Piping Network. *IEEE Trans. Ind. Electron.* **2022**, *69*, 2345–2356.
32. Liu, W.; Chau, K.T.; Wang, H.; et al. Long-Range Wireless Power Drive Using Magnetic Extender. *IEEE Trans. Transp. Electrif.* **2023**, *9*, 1897–1909.
33. Jiang, C.; Chau, K.T.; Ching, T.W.; et al. Time-Division Multiplexing Wireless Power Transfer for Separately Excited DC Motor Drives. *IEEE Trans. Magn.* **2017**, *53*, 1–5.
34. Jiang, C.; Chau, K.T.; Lee, C.H.T.; et al. A Wireless Servo Motor Drive with Bidirectional Motion Capability. *IEEE Trans. Power Electron.* **2019**, *34*, 12001–12010.
35. Han, W.; Chau, K.T.; Hua, Z.; et al. Compact Wireless Motor Drive Using Orthogonal Bipolar Coils for Coordinated Operation of Robotic Arms. *IEEE Trans. Magn.* **2022**, *58*, 1–8.
36. Liu, H.; Zhou, H.; Deng, Q.; et al. A Wireless DC Motor Drive Using LCCC-CCL Compensated Network with Bidirectional Motion Capability. *IEEE Trans. Circuits Syst. I* **2022**, *69*, 4714–4725.
37. Ayaz, E.; Altun, O.; Polat, H.; et al. Concurrent Wireless Power Transfer and Motor Drive System with a Single Converter. *IEEE J. Emerg. Sel. Top. Ind. Electron.* **2023**, *4*, 409–418.

38. Chen, X.F.; Tse, C.K.; Jiang, C.Q.; et al. Soft Switching Based Design of a Single-Stage Wireless DC Motor Drive System for Typical Mechanical Loads. *IEEE Trans. Ind. Appl.* **2024**, *60*, 8976–8987.
39. Chen, X.F.; Tse, C.K.; Chen, Q. Electrolytic Capacitorless Wireless DC Motor Drive System with Delta-Sigma Modulation. In Proceedings of the IEEE Energy Conversion Congress and Exposition (ECCE), Phoenix, AZ, USA, 20–24 October 2024; pp. 2325–2327.
40. Chen, X.F.; Tse, C.K.; Wang, X.; et al. Electrolytic Capacitor-Less Wireless Motor Drive System with Delta-Sigma Modulation. *IEEE Trans. Ind. Electron.* **2025**, *72*, 12355–12367.
41. Babaki, A.; Vaez-Zadeh, S.; Zakerian, A.; et al. Analysis and Control of Wireless Motor Drives with a Single Inverter in Primary Side. *IEEE Trans. Energy Convers.* **2021**, *36*, 930–939.
42. Wang, H.; Chau, K.T.; Lee, C.H.T.; et al. Design, Analysis, and Implementation of Wireless Shaded-Pole Induction Motors. *IEEE Trans. Ind. Electron.* **2021**, *68*, 6493–6503.
43. Wang, H.; Chau, K.T.; Lee, C.H.T.; et al. Wireless Shaded-Pole Induction Motor with Half-Bridge Inverter and Dual-Frequency Resonant Network. *IEEE Trans. Power Electron.* **2021**, *36*, 13536–13545.
44. Ayaz, E.; Altun, O.; Keysan, O. Carrier Phase Shift Method of SPWM for Concurrent Wired and Wireless Power Transfer Systems. *IEEE Trans. Ind. Electron.* **2023**, *70*, 8645–8654.
45. Ayaz, E.; Altun, O.; Keysan, O. Variable Carrier Phase-Shift Method for Integrated Contactless Field Excitation System of Electrically Excited Synchronous Motors. *IEEE Trans. Power Electron.* **2023**, *38*, 13243–13253.
46. Jin, P.; Chang, L.; Liu, Y.; et al. Design and Implementation of Novel Rotor Side Brushless Controller with Bidirectional Wireless Power Transmission for Doubly-Fed Machine. *IEEE Trans. Ind. Electron.* **2024**, *71*, 183–193.
47. Ding, W.; Li, K.; Yuan, J.; et al. Wireless Power Transmission-Based In-Wheel Switched Reluctance Motor Drive System with an X-Type Converter. *IEEE Trans. Energy Convers.* **2023**, *38*, 450–462.
48. Jiang, C.; Chau, K.T.; Liu, C.; et al. Design and Analysis of Wireless Switched Reluctance Motor Drives. *IEEE Trans. Ind. Electron.* **2019**, *66*, 245–254.
49. Jiang, C.; Chau, K.T.; Liu, C.; et al. An LCC-Compensated Multiple-Frequency Wireless Motor System. *IEEE Trans. Ind. Inf.* **2019**, *15*, 6023–6034.
50. Han, W.; Chau, K.T.; Hua, Z.; et al. An Integrated Wireless Motor System Using Laminated Magnetic Coupler and Commutative-Resonant Control. *IEEE Trans. Ind. Electron.* **2022**, *69*, 4342–4352.
51. Wang, H.; Chau, K.T.; Lee, C.H.T.; et al. Design and Analysis of Wireless Resolver for Wireless Switched Reluctance Motors. *IEEE Trans. Ind. Electron.* **2023**, *70*, 2221–2230.
52. Li, K.; Ding, W.; Yuan, J.; et al. A Decoupled Multichannel Based Wireless SRM System with Tunable Compensation Network and Multifrequency Pulse Density Control. *IEEE Trans. Ind. Electron.* **2024**, *71*, 1468–1480.
53. Fang, L.; Zhou, H.; Hu, W.; et al. Design of Wireless Individual-Drive System for Variable-Reluctance Stepping Motor. *IEEE Trans. Circuits Syst. II* **2022**, *69*, 2141–2145.
54. Wang, H.; Chau, K.T.; Liu, W.; et al. Design and Control of Wireless Permanent-Magnet Brushless DC Motors. *IEEE Trans. Energy Convers.* **2023**, *38*, 2969–2979.
55. Madzharov, N.; Ilarionov, R.; Petkov, V.; et al. Inductive Power Transfer Systems for Rotating Applications. In Proceedings of the International Exhibition and Conference on Power Electronics, Intelligent Motion, Renewable Energy and Energy Management, Nuremberg, Germany, 5–7 June 2018; pp. 1–8.
56. Abdolkhani, A.; Hu, A.P.; Nair, N.C.K. Modelling and Parameters Identification of Through-Hole Type Wind Turbine Contactless Sliprings. *Engineering* **2012**, *4*, 272–283.
57. Abdolkhani, A.; Hu, A.P. Face to Face Through-Hole Contactless Slipring System for Rotary Applications. *Int. J. Adv. Res. Electr. Electron. Instrum. Eng.* **2013**, *2*, 4227–4286.
58. He, G.; Chen, Q.; Ren, X.; et al. Modeling and Design of Contactless Sliprings for Rotary Applications. *IEEE Trans. Ind. Electron.* **2019**, *66*, 4130–4140.
59. Papastergiou, K.D.; Macpherson, D.E. Contact-less Transfer of Energy by Means of a Rotating Transformer. In Proceedings of the IEEE International Symposium on Industrial Electronics, Dubrovnik, Croatia, 20–23 June 2005; pp. 1735–1740.
60. Papastergiou, K.D.; Macpherson, D.E. An Airborne Radar Power Supply with Contactless Transfer of Energy—Part I: Rotating Transformer. *IEEE Trans. Ind. Electron.* **2007**, *54*, 2874–2884.
61. Smeets, J.; Encica, L.; Lomonova, E.A. Comparison of Winding Topologies in a Pot Core Rotating Transformer. In Proceedings of the 12th International Conference on Optimization of Electrical and Electronic Equipment, Brasov, Romania, 20–22 May 2010; pp. 103–110.
62. Abdolkhani, A.; Hu, A.P. A Novel Detached Magnetic Coupling Structure for Contactless Power Transfer. In Proceedings of the 37th Annual Conference of the IEEE Industrial Electronics Society, Melbourne, VIC, Australia, 7–10 November 2011; pp. 1103–1108.

63. Bortis, D.; Fässler, L.; Looser, A.; et al. Analysis of Rotary Transformer Concepts for High-Speed Applications. In Proceedings of the 28th IEEE Applied Power Electronics Conference and Exposition, Long Beach, CA, USA, 17–21 March 2013; pp. 3262–3269.
64. Abdolkhani, A.; Hu, A.P.; Nair, N.K.C. A Double Stator Through-Hole Type Contactless Slipring for Rotary Wireless Power Transfer Applications. *IEEE Trans. Energy Convers.* **2014**, *29*, 426–434.
65. Raminosoa, T.; Wiles, R.H.; Wilkins, J. Novel Rotary Transformer Topology with Improved Power Transfer Capability for High-Speed Applications. *IEEE Trans. Ind. Appl.* **2020**, *56*, 277–286.
66. Ditze, S.; Endruschat, A.; Schriefer, T.; et al. Inductive Power Transfer System with a Rotary Transformer for Contactless Energy Transfer on Rotating Applications. In Proceedings of the IEEE International Symposium on Circuits and Systems, Montreal, QC, Canada, 22–25 May 2016; pp. 1622–1625.
67. Wang, N.; Zhao, Y.; Li, C.; et al. Design, Manufacture and Experimental Verification of Contactless Power Supply Coupler for Rotary Wireless Sensor Node of Water-Lubricated Bearing. *IEEE Trans. Instrum. Meas.* **2023**, *72*, 1–11.
68. He, G.; Chen, Q.; Ren, X.; et al. LL-Delta Structure for CS Featuring High-PTC. *IET Power Electron.* **2019**, *12*, 2543–2550.
69. Abdolkhani, A.; Hu, A.P. Improved Coupling Design of Contactless Slipring for Rotary Applications. *IEEE J. Emerg. Sel. Top. Power Electron.* **2015**, *3*, 288–295.
70. Abdolkhani, A.; Hu, A.P. A Contactless Slipring System by Means of Axially Travelling Magnetic Field. In Proceedings of the IEEE Energy Conversion Congress and Exposition, Raleigh, NC, USA, 15–20 September 2012; pp. 1796–1803.
71. Abdolkhani, A.; Hu, A.P. A Contactless Slipring System Based on Axially Travelling Magnetic Field. *IEEE J. Emerg. Sel. Top. Power Electron.* **2015**, *3*, 280–287.
72. Abdolkhani, A.; Hu, A.P.; Covic, G.; et al. Contactless Slipring System Based on Rotating Magnetic Field Principle for Rotary Applications. In Proceedings of the IEEE Energy Conversion Congress and Exposition, Denver, CO, USA, 15–19 September 2013; pp. 2566–2573.
73. Abdolkhani, A.; Hu, A.P.; Covic, G.A.; et al. Through-Hole Contactless Slipring System Based on Rotating Magnetic Field for Rotary Applications. *IEEE Trans. Ind. Appl.* **2014**, *50*, 3644–3655.
74. Shin, J.; Shin, S.; Kim, Y.; et al. Design and Implementation of Shaped Magnetic-Resonance-Based Wireless Power Transfer System for Roadway-Powered Moving Electric Vehicles. *IEEE Trans. Ind. Electron.* **2014**, *61*, 1179–1192.
75. Choi, S.Y.; Gu, B.W.; Jeong, S.Y.; et al. Advances in Wireless Power Transfer Systems for Roadway-Powered Electric Vehicles. *IEEE J. Emerg. Sel. Top. Power Electron.* **2015**, *3*, 18–36.
76. Huh, J.; Lee, S.W.; Lee, W.Y.; et al. Narrow-Width Inductive Power Transfer System for Online Electrical Vehicles. *IEEE Trans. Power Electron.* **2011**, *26*, 3666–3679.
77. Choi, S.Y.; Jeong, S.Y.; Gu, B.W.; et al. Ultraslim S-Type Power Supply Rails for Roadway-Powered Electric Vehicles. *IEEE Trans. Power Electron.* **2015**, *30*, 6456–6468.
78. Wang, Z.; Cui, S.; Han, S.; et al. A Novel Magnetic Coupling Mechanism for Dynamic Wireless Charging System for Electric Vehicles. *IEEE Trans. Veh. Technol.* **2018**, *67*, 124–133.
79. Miller, J.M.; Onar, O.C.; White, C.; et al. Demonstrating Dynamic Wireless Charging of an Electric Vehicle: The Benefit of Electrochemical Capacitor Smoothing. *IEEE Power Electron. Mag.* **2014**, *1*, 12–24.
80. Guo, Y.; Wang, L.; Zhu, Q.; et al. Switching-On Modeling and Analysis of Dynamic Wireless Charging System Used for Electric Vehicles. *IEEE Trans. Ind. Electron.* **2016**, *63*, 658–6579.
81. Tavakoli, R.; Pantic, Z. Analysis, Design, and Demonstration of a 25-kW Dynamic Wireless Charging System for Roadway Electric Vehicle. *IEEE J. Emerg. Sel. Top. Power Electron.* **2018**, *6*, 1378–1393.
82. Liu, Y.; Mai, R.; Liu, D.; et al. Efficiency Optimization for Wireless Dynamic Charging System with Overlapped DD Coil Arrays. *IEEE Trans. Power Electron.* **2018**, *33*, 2832–2846.
83. Gao, W.; Chen, Q.; Ren, X.; et al. An Elliptical Magnetic Field-Orientated Control for Interoperability and Misalignment Tolerance in Inductive Power Transfer. In Proceedings of the IEEE PELS Workshop on Emerging Technologies, Montreal, QC, Canada, 3–7 June 2018; pp. 1–6.
84. Gao, J. Traveling Magnetic Field for Homogeneous Wireless Power Transmission. *IEEE Trans. Power Del.* **2007**, *22*, 507–514.
85. Covic, G.A.; Boys, J.T.; Kissin, M.L.G.; et al. A Three-Phase Inductive Power Transfer System for Roadway-Powered Vehicles. *IEEE Trans. Ind. Electron.* **2007**, *54*, 3370–3378.
86. Matsumoto, H.; Neba, Y.; Ishizaka, K.; et al. Model for a Three-Phase Contactless Power Transfer System. *IEEE Trans. Power Electron.* **2011**, *26*, 2676–2687.
87. Li, Y.; Hu, J.; Lin, T.; et al. A New Coil Structure and Its Optimization Design with Constant Output Voltage and Constant Output Current for Electric Vehicle Dynamic Wireless Charging. *IEEE Trans. Ind. Inf.* **2019**, *15*, 5244–5256.
88. Nagendra, G.R.; Covic, G.A.; Boys, J.T. Sizing of Inductive Power Pads for Dynamic Charging of EVs on IPT Highways. *IEEE Trans. Transp. Electrif.* **2017**, *3*, 405–417.

89. Hou, J.; Chen, Q.; Zhang, Z.; et al. Analysis of Output Current Characteristics for Higher Order Primary Compensation in Inductive Power Transfer Systems. *IEEE Trans. Power Electron.* **2018**, *33*, 6807–6821.
90. Zhang, Y.; Chen, Q.; Ren, X.; et al. Design of S/P Compensated IPT System Considering Parameter Variations in Consideration of ZVS Achievement. In Proceedings of the IEEE Energy Conversion Congress and Exposition, Milwaukee, WI, USA, 18–22 September 2016; pp. 1–6.
91. Hou, J.; Chen, Q.; Wong, S.C.; et al. Analysis and Control of Series/Series-Parallel Compensated Resonant Converter for Contactless Power Transfer. *IEEE J. Emerg. Sel. Top. Power Electron.* **2015**, *3*, 124–136.
92. Feng, H.; Cai, T.; Duan, S.; et al. An LCC-Compensated Resonant Converter Optimized for Robust Reaction to Large Coupling Variation in Dynamic Wireless Power Transfer. *IEEE Trans. Ind. Electron.* **2016**, *63*, 6591–6601.
93. Mai, R.; Chen, Y.; Li, Y.; et al. Inductive Power Transfer for Massive Electric Bicycles Charging Based on Hybrid Topology Switching with a Single Inverter. *IEEE Trans. Power Electron.* **2017**, *32*, 5897–5906.
94. Xu, F.; Wong, S.C.; Tse, C.K. Overall Loss Compensation and Optimization Control in Single-Stage Inductive Power Transfer Converter Delivering Constant Power. *IEEE Trans. Power Electron.* **2022**, *37*, 1146–1158.
95. Chen, X.F.; Tse, C.K.; Jiang, C. Control and Soft Switching Analysis of a Single-Stage Wireless DC Motor Drive System. In Proceedings of the IEEE 11th International Conference on Power Electronics (ECCE Asia), Jeju Island, Korea, 22–25 May 2023; pp. 1018–1024.
96. Lu, J.; Zhu, G.; Wang, H.; et al. Sensitivity Analysis of Inductive Power Transfer Systems with Voltage-Fed Compensation Topologies. *IEEE Trans. Veh. Technol.* **2019**, *68*, 4502–4513.
97. Li, S.; Li, W.; Deng, J.; et al. A Double-Sided LCC Compensation Network and Its Tuning Method for Wireless Power Transfer. *IEEE Trans. Veh. Technol.* **2015**, *64*, 2261–2273.
98. Schweizer, M.; Kolar, J.W. Design and Implementation of a Highly Efficient Three-Level T-Type Converter for Low-Voltage Applications. *IEEE Trans. Power Electron.* **2013**, *28*, 899–907.
99. Huang, J.; Corzine, K.A. Extended Operation of Flying Capacitor Multilevel Inverters. *IEEE Trans. Power Electron.* **2006**, *21*, 140–147.
100. Nabae, A.; Takahashi, I.; Akagi, H. A New Neutral-Point-Clamped PWM Inverter. *IEEE Trans. Ind. Appl.* **1981**, *IA-17*, 518–523.
101. Bruckner, T.; Bernet, S.; Guldner, H. The Active NPC Converter and Its Loss-Balancing Control. *IEEE Trans. Ind. Electron.* **2005**, *52*, 855–868.
102. Hammond, P.W. A New Approach to Enhance Power Quality for Medium Voltage AC Drives. *IEEE Trans. Ind. Appl.* **1997**, *33*, 202–208.
103. Akagi, H. Classification, Terminology, and Application of the Modular Multilevel Cascade Converter (MMCC). *IEEE Trans. Power Electron.* **2011**, *26*, 3119–3130.
104. Wiechmann, E.P.; Aqueveque, P.; Burgos, R.; et al. On the Efficiency of Voltage Source and Current Source Inverters for High-Power Drives. *IEEE Trans. Ind. Electron.* **2008**, *55*, 1771–1782.
105. Amorim Torres, R.; Dai, H.; Lee, W.; et al. Current-Source Inverter Integrated Motor Drives Using Dual-Gate Four-Quadrant Wide-Bandgap Power Switches. *IEEE Trans. Ind. Appl.* **2021**, *57*, 5183–5198.
106. Wu, B.; Narimani, M. *High-Power Converters and AC Drives*; Wiley: Hoboken, NJ, USA, 2017.
107. Chau, K.T. *Electric Vehicle Machines and Drives: Design, Analysis and Application*; Wiley-IEEE Press: Hoboken, NJ, USA, 2015.
108. Ding, W.; Yang, S.; Hu, Y. Performance Improvement for Segmented-Stator Hybrid-Excitation SRM Drives Using an Improved Asymmetric Half-Bridge Converter. *IEEE Trans. Ind. Electron.* **2019**, *66*, 898–909.
109. Barnes, M.; Pollock, C. Power Electronic Converters for Switched Reluctance Drives. *IEEE Trans. Power Electron.* **1998**, *13*, 1100–1111.
110. Pollock, C.; Williams, B.W. Power Convertor Circuits for Switched Reluctance Motors with the Minimum Number of Switches. *IEE Proc. B* **1990**, *137*, 373–384.
111. Mir, S.; Husain, I.; Elbuluk, M.E. Energy-Efficient C-Dump Converters for Switched Reluctance Motors. *IEEE Trans. Power Electron.* **1997**, *12*, 912–921.
112. Krishnan, R.; Materu, P.N. Analysis and Design of a Low-Cost Converter for Switched Reluctance Motor Drives. *IEEE Trans. Ind. Appl.* **1993**, *29*, 320–327.
113. Ray, W.F.; Lawrenson, P.J.; Davis, R.M.; et al. High-Performance Switched Reluctance Brushless Drives. *IEEE Trans. Ind. Appl.* **1986**, *IA-22*, 722–730.
114. Qu, X.; Jing, Y.; Han, H.; et al. Higher Order Compensation for Inductive Power-Transfer Converters with Constant-Voltage or Constant-Current Output Combating Transformer Parameter Constraints. *IEEE Trans. Power Electron.* **2017**, *32*, 394–405.
115. Liu, Y.C.; Zhang, J.; Tse, C.K.; et al. General Pathways to Higher Order Compensation Circuits for IPT Converters via Sensitivity Analysis. *IEEE Trans. Power Electron.* **2021**, *36*, 9897–9906.

116. Hou, J.; Chen, Q. Optimization of Current Source Inverter in Inductive Power Transfer Systems. In Proceedings of the 9th International Conference on Power Electronics (ECCE Asia), Nanjing, China, 29 November–2 December 2020; pp. 2969–2973.
117. Xu, Y.; Wang, Z.; Liu, P.; et al. Current-Fed Isolated Three-Phase Matrix-Type Grid Inverter with Soft-Switching Capability. *IEEE Trans. Ind. Electron.* **2022**, *69*, 3292–3302.
118. Kim, Y.J.; Ha, D.; Chappell, W.J.; et al. Selective Wireless Power Transfer for Smart Power Distribution in a Miniature-Sized Multiple-Receiver System. *IEEE Trans. Ind. Electron.* **2016**, *63*, 1853–1862.
119. Zhang, Y.; Lu, T.; Zhao, Z.; et al. Selective Wireless Power Transfer to Multiple Loads Using Receivers of Different Resonant Frequencies. *IEEE Trans. Power Electron.* **2015**, *30*, 6001–6005.
120. Xia, C.; Ren, S.; Chen, R.; et al. Inductive Power and Signal Synchronous Transmission Based on Parallel Paths of Fundamental Wave and Harmonic Wave. *Autom. Electr. Power Syst.* **2018**, *42*, 169–175. (In Chinese)
121. Zhang, Z.; Li, X.; Pang, H.; et al. Multiple-Frequency Resonating Compensation for Multichannel Transmission of Wireless Power Transfer. *IEEE Trans. Power Electron.* **2021**, *36*, 5169–5180.
122. Guo, M.; Chen, Q.; Chen, X.F.; et al. Analysis and Utilization of the Harmonic in Contactless Slipring System. In Proceedings of the 9th International Conference on Power Electronics (ECCE Asia), Nanjing, China, 29 November–2 December 2020; pp. 2997–3002.
123. Li, H.L.; Hu, A.P.; Covic, G.A. A Direct AC-AC Converter for Inductive Power-Transfer Systems. *IEEE Trans. Power Electron.* **2012**, *27*, 661–668.
124. Weerasinghe, S.; Madawala, U.K.; Thrimawithana, D.J. A Matrix Converter-Based Bidirectional Contactless Grid Interface. *IEEE Trans. Power Electron.* **2017**, *32*, 1755–1766.
125. Samanta, S.; Rathore, A.K. A New Inductive Power Transfer Topology Using Direct AC-AC Converter with Active Source Current Waveshaping. *IEEE Trans. Power Electron.* **2018**, *33*, 5565–5577.
126. Moghaddami, M.; Sarwat, A.I. Single-Phase Soft-Switched AC-AC Matrix Converter with Power Controller for Bidirectional Inductive Power Transfer Systems. *IEEE Trans. Ind. Appl.* **2018**, *54*, 3760–3770.
127. Bac, N.X.; Vilathgamuwa, D.M.; Madawala, U.K. A Matrix Converter Based Inductive Power Transfer System. In Proceedings of the IEEE Conference on Power and Energy, Ho Chi Minh City, Vietnam, 12–14 December 2012; pp. 509–514.
128. Xuan Bac, N.; Vilathgamuwa, D.M.; Madawala, U.K. A SiC-Based Matrix Converter Topology for Inductive Power Transfer System. *IEEE Trans. Power Electron.* **2014**, *29*, 4029–4038.
129. Hayashi, Y.; Motoyama, H.; Takeshita, T. Wireless Power Transfer System Using Three-Phase to Single-Phase Matrix Converter. In Proceedings of the International Conference on Power Electronics (ECCE Asia), Niigata, Japan, 20–24 May 2018; pp. 356–362.
130. Xiao, Y.; Liu, C. Direct Load Voltage Control for Electrolytic Capacitorless Wireless Power Transfer System without DC/DC Converter. *IEEE Trans. Ind. Electron.* **2021**, *68*, 8039–8048.
131. Mirković, N.R.; Stojić, D.M.; Delgado, A.; et al. Novel Three Phase to Single Phase Matrix Converter Modulation Strategy for Bidirectional Inductive Power Transfer. *IEEE Trans. Power Electron.* **2023**, *38*, 14830–14846.
132. Wei, Y.; Wu, F.; Wu, S.; et al. Improved Modulation Strategy for Three-Phase Matrix Converter-Based WPT System. *IEEE Trans. Transp. Electrif.* **2024**, *10*, 3396–3406.
133. Moghaddami, M.; Anzalchi, A.; Sarwat, A.I. Single-Stage Three-Phase AC-AC Matrix Converter for Inductive Power Transfer Systems. *IEEE Trans. Ind. Electron.* **2016**, *63*, 6613–6622.
134. Kolar, J.W.; Friedli, T.; Rodriguez, J.; et al. Review of Three-Phase PWM AC-AC Converter Topologies. *IEEE Trans. Ind. Electron.* **2011**, *58*, 4988–5006.
135. Empringham, L.; Kolar, J.W.; Rodriguez, J.; et al. Technological Issues and Industrial Application of Matrix Converters: A Review. *IEEE Trans. Ind. Electron.* **2013**, *60*, 4260–4271.
136. Jin, P.; Cao, C.; Guo, Y.; et al. A Novel SVM Strategy to Reduce Current Stress of 3-3 AC/AC HFLMC. *IEEE Trans. Ind. Electron.* **2026**, *73*, 6–15.
137. Chen, X.F.; Tse, C.K.; Chen, Q. Improved Modulation Strategy for Single-Phase Integrated Wireless Charging System. In Proceedings of the IEEE 16th International Symposium on Power Electronics for Distributed Generation Systems (PEDG), Nanjing, China, 22–25 June 2025; pp. 1–6.
138. Kumar, J.; Samanta, S. A Single-Stage Universal Input Wireless Inductive Power Transfer System with V2G Capability. *IEEE J. Emerg. Sel. Top. Ind. Electron.* **2024**, *5*, 1017–1029.
139. Wang, R.; Wang, F.; Boroyevich, D.; et al. A High Power Density Single-Phase PWM Rectifier with Active Ripple Energy Storage. *IEEE Trans. Power Electron.* **2011**, *26*, 1430–1443.
140. Wang, H.; Liu, Y.; Wang, H. On the Practical Design of a Two-Terminal Active Capacitor. *IEEE Trans. Power Electron.* **2019**, *34*, 10006–10020.
141. She, X.; Huang, A.Q.; Burgos, R. Review of Solid-State Transformer Technologies and Their Application in Power Distribution Systems. *IEEE J. Emerg. Sel. Top. Power Electron.* **2013**, *1*, 186–198.

142. Huber, J.E.; Kolar, J.W. Applicability of Solid-State Transformers in Today's and Future Distribution Grids. *IEEE Trans. Smart Grid* **2019**, *10*, 317–326.
143. Wang, J.; Li, Y.; Han, Y. Integrated Modular Motor Drive Design with GaN Power FETs. *IEEE Trans. Ind. Appl.* **2015**, *51*, 3198–3207.
144. Jahns, T.M.; Sarlioglu, B. The Incredible Shrinking Motor Drive: Accelerating the Transition to Integrated Motor Drives. *IEEE Power Electron. Mag.* **2020**, *7*, 18–27.
145. Casaucao Tenllado, I.; Triviño Cabrera, A.; Lin, Z. Simultaneous Wireless Power and Data Transfer for Electric Vehicle Charging: A Review. *IEEE Trans. Transp. Electrif.* **2024**, *10*, 4542–4570.
146. Fan, Y.; Hu, H.; Sun, Y.; et al. A Simultaneous Wireless Power and Coil Inductance Insensitive Data Transfer System for Rotary Structures. *IEEE Trans. Power Electron.* **2024**, *39*, 6526–6536.
147. Qiu, W.; Zhao, X.; Tyrrell, A.; et al. Application of Artificial Intelligence-Based Technique in Electric Motors: A Review. *IEEE Trans. Power Electron.* **2024**, *39*, 13543–13568.